REFRACTORY AND SEMI-VOLATILE ORGANICS AT THE SURFACE OF COMET 67P/CHURYUMOV-GERASIMENKO: INSIGHTS FROM THE VIRTIS/ROSETTA IMAGING SPECTROMETER

E. Quirico[1] L. V. Moroz[2,3], B. Schmitt[1], G. Arnold[3], M. Faure[1], P. Beck[1], L. Bonal[1], M. Ciarniello[4], F. Capaccioni[4], G. Filacchione[4], S. Erard[5], C. Leyrat[5], D. Bockelée-Morvan[5], A. Zinzi[4], E. Palomba[4], P. Drossart[5], F. Tosi[4], M. T. Capria[4], M. C. De Sanctis[4], A. Raponi[4], S. Fonti[6], F. Mancarella[6], V. Orofino[6], A. Barucci[5], M. I. Blecka[7], B. Carlson[8], D. Despan[5], A. Faure[1], Fornasier[5] S., M. S. Gudipati[8], A. Longobardo[4], K. Markus[3], V. Menella[9], F. Merlin[5], G. Piccioni[4], B. Rousseau[5], F. Taylor[10], and the Rosetta VIRTIS team.

(1) Université Grenoble Alpes, CNRS, Institut de Planétologie et Astrophysique de Grenoble (IPAG), UMR 5274, Grenoble F-38041 France

(2) University of Postdam, Germany

(3) German Aerospace Center (DLR), Berlin, Germany

(4) IAPS-INAF, via del fosso del cavaliere, 100, 00133, Rome, Italy

(5) LESIA, Observatoire de Paris, PSL Research University, CNRS, Sorbonne Universités, UPMC Univ. Paris 06, Univ. Paris Diderot, Sorbonne Paris Cité

(6) Dipartimento di Matematica e Fisica "E. De Giorgi", Università del Salento, Lecce, Italy

(7) Space Research Centre, Polish Academy of Sciences, Warsaw, Poland

(8) NASA Jet Propulsion Laboratory, Pasadena, CA 91109, USA

(9) Osservatorio di Capodimonte, INAF, Napoli, Italy.

(10) Department of Physics, Oxford University, Oxford, UK

To whom correspondence should be addressed:

Eric Quirico

E-mail: eric.quirico@obs.ujf-grenoble.fr

Tel +33 4 76 51 41 56

ABSTRACT

The VIRTIS (Visible, Infrared and Thermal Imaging Spectrometer) instrument onboard the Rosetta spacecraft has provided extensive spectral mapping of the surface of comet 67P/Churyumov-Gerasimenko, in the range 0.3-5 μm. The reflectance spectra collected across the surface display a low reflectance factor through the whole spectral range, two spectral slopes in the visible and the near-infrared ranges, and a broad band centered at 3.2 μm. The first two of these characteristics are typical of dark small bodies of the Solar System, and in this respect their interpretation in terms of composition is difficult. Solar wind irradiation may modify the structure and composition of surface materials, and there is no univocal assignment for those spectra devoid of vibrational bands. In order to circumvent these problems, we developed an analysis by constraining the nature of cometary materials from the study of cometary grains analyzed in the laboratory and by considering results on surface rejuvenation and solar wind processing provided by the OSIRIS and ROSINA instruments, respectively. Our results show that (1) The low albedo of comet 67P/CG is accounted for by a dark refractory polyaromatic carbonaceous component mixed up with opaque minerals. VIRTIS data do not provide direct insights into the nature of these opaque minerals. However, according to the composition of cometary grains analyzed in the laboratory, we infer they consist of Fe-Ni alloys and ~FeS sulfides. (2) A semi-volatile component, consisting of a complex mix of low weight molecular species not volatilized at T~220 K, is likely a major carrier of the 3.2 μm band. Water ice has a significant contribution to this feature in the neck region, but not in other regions of the comet. COOH in carboxylic acids is the only chemical group that encompasses the broad width of this feature. It appears as a highly plausible candidate, along with the NH_4^+ ion. (3) Photolytic/thermal residues, produced in the laboratory from interstellar ice analogs, appear as potential interesting spectral analogs. (4) No hydrated minerals were identified and our data support the lack of generic links with the CI, CR and CM primitive chondrites. This concerns in particular the Orgueil chondrite, which had been suspected to have a cometary origin. (5) The comparison between fresh and aged terrains revealed no effect of solar wind irradiation on the 3.2 μm band. This is consistent with the presence of efficient resurfacing processes, such as dust transport from the interior to the surface as revealed by the OSIRIS camera.

1. INTRODUCTION

The surfaces of comets and other small bodies of our Solar System are at the convergence of several key issues. Systematic observational surveys of small bodies focus on their surfaces, which constitute the only way to infer their bulk composition. They provide as well a statistical view of compositional diversity and help explore the dynamical evolution of the early Solar System and the so-called asteroid-comet continuum (Hughes and Armitage, 2010; Walsh et al., 2011). Cometary surfaces are also exposed to solar wind irradiation, but are efficiently shielded by their dusty coma when they approach the Sun, and they are subjected to resurfacing processes that can partly or fully rejuvenate them. In this respect, they might be more primitive (i.e. not altered by space weather) than other minor bodies devoid of surface rejuvenation and might help understand the effect of space weathering on dark surfaces. Comets also spread dust in the interplanetary medium that is eventually accreted by Earth as stratospheric interplanetary dust particles (IDPs) and Antarctic micrometeorites (AMMs). The analysis in the laboratory of these particles provides insightful clues on the refractory component of comets, and makes it possible to investigate the connection with astronomical objects.

The Rosetta mission opens unprecedented perspectives on these issues. Comet 67P/Churyumov-Gerasimenko has been escorted since August 2014 by the Rosetta spacecraft and its lander Philae, which touched down onto its surface on November 14 2014. In situ measurements from the orbiter have been operated when the comet was weakly active at 4 AU, and have been pursued after perihelion. The evolution of surface composition and morphology are thus being studied, and thus should provide the spectral properties of *pristine* cometary material (*pristine* defined as "unprocessed by space weathering").

The spectral properties of comet 67P/CG surface have been investigated by means of the VIRTIS instrument aboard the Rosetta orbiter (Visible InfraRed Thermal Imaging Spectrometer). This instrument comprises two channels: (i) a high spectral resolution single-pixel spectrometer, mainly devoted to the study of the coma properties in the 1.88-5.03 µm spectral range (channel H), and (ii) an imaging spectrometer producing hyperspectral images of the target in the 0.3-5.1 µm spectral range with an angular resolution of 250 µrad x 250 µrad (channel M) (Coradini et al., 2007). 67P/CG spectra are characterized by (1) a red slope in the visible, (2) a weaker reddish slope in the near-infrared (0.8-2.7 µm), and (3) a reflectance factor that does not exceed 6% over the whole spectral range. They thus reveal a dark surface in both the visible and near-infrared ranges (normal albedo ~6 % at 0.55 µm). Extracted Hapke parameters (single scattering albedo, scattering parameter) are basically similar to those collected on comets Tempel 1, Hartley 2 and Borelly (Ciarnello et al., 2015; Fornasier et al., 2015). However, a broad absorption band centered at 3.2 µm has been detected for the first time (Capaccioni et al. 2015). The surface has also been extensively characterized by the OSIRIS camera (Sierks et al., 2015) in terms of morphology from 4 AU to perihelion, evidencing two main types of terrains as (1) rocky consolidated terrains, which often display evidence of thermal fatigue, and (2) fine-grained regions, with fresh deposits (Thomas et al., 2015; El-Maarry et al., 2015).

The interpretation of the reflectance spectra of 67P/CG in terms of surface composition is the subject of this article. Generally speaking, the interpretation of featureless reflectance spectra of dark surfaces of the Solar System is a challenging task, because it relies mostly on spectral slopes and absolute reflectance, which do not bear unequivocal information. As different materials may display similar absorption properties, it is necessary to circumvent this bias by inferring the most plausible analogs. In this study, we present an interpretation constrained by knowledge of the composition of primitive meteorites, IDPs and AMMs. We found that fair analogs of cometary refractory carbon are samples of terrestrial sedimentary organic matter, as coals and bitumens. Laboratory reflectance measurements of

these analogs and of primitive carbonaceous chondrites of the CI, CM and CR classes were collected and compared to 67P/CG spectra, under similar observation geometry. These data provided new insights on the interpretation of the low reflectance in the visible and near-infrared ranges, and on the link with carbonaceous chondrites. The interpretation of the 3.2 µm band, which is observed neither in IDPs and AMMs nor in carbonaceous chondrites, has been thoroughly investigated through spectral mappings of five regions of the comets well characterized in terms of morphology. This made it possible to discuss the effect of solar wind irradiation on the spectral characteristics of this band.

The paper is organized as follows: (i) Section 2 presents VIRTIS observations, emphasizing the mapping of the 3.2 µm band in five regions. (ii) Section 3 presents the samples that have been used as analogs of the carbon-rich surface of 67P/CG. The relevancy of coal samples is addressed in detail. (iii) Section 4 presents laboratory measurements on coal and coal tar samples and primitive meteorites. (iv) Section 5 reports discussion on the spectral properties of coals and coal tars, proposes an interpretation of the low reflectance, reports a detailed spectroscopic interpretation of the 3.2 µm band and finally discusses the impact of solar wind irradiation.

2. VIRTIS-M OBSERVATIONS

2.1 Data reduction

VIRTIS-M provided for each pixel the radiance factor *I/F* as a function of wavelength (λ) under geometrical conditions characterized by the *i*, *e* and *g* angles (incidence, emergence and phase angles, respectively). *I* and πF are here the nucleus radiance and the solar irradiance at normal incidence, respectively. Radiance factor data were corrected for thermal emission using the surface temperature maps derived by Tosi et al. (in preparation) for each data cube. For this purpose, a constant emissivity ε=0.95 over the wavelength range <4.5 µm (for T<220 K) was used, and the Kirrchhoff's law was applied iteratively. Calculations show that the resulting reflected radiance spectra below 4.5 µm are weakly sensitive to surface temperature. At longer wavelengths, the higher sensitivity to temperature leads to large variations of the continuum slope. In this publication, we mostly restrict the analysis to the spectrum at wavelengths <4.5 µm. Different instrumental artifacts were fixed in order to avoid spectral distortions in specific area, e.g. limb, high albedo contrast or shadowed areas. The REFF reflectance factor as defined by Hapke (1993) was obtained through the following equation:

$$\mathrm{REFF}(\mathrm{i},\mathrm{e},\mathrm{g},\lambda) = \frac{\mathrm{I}(\mathrm{i},\mathrm{e},\mathrm{g},\lambda)}{F}\frac{1}{\cos(\mathrm{i})}$$

2.2 Photometry

Typical reflectance spectra are displayed in Figure 1a. Mean reflectance spectra for i=0 and e=30° have been calculated with the procedure defined by Ciarnello et al. (2015), for four macro-regions defined as "head", "neck", "body" and "bottom". The spectra exhibit the visible and infrared slope, the 3.2 µm band and are very close to each other with a reflectance factor that does not exceed 0.06 throughout the 0.4-4.7 µm range. Figure 1a also displays representative reflectance spectra for the brightest and darkest area in the same geometrical conditions. The variation range of REFF remains narrow (0.046 ± 0.008 at ~2.7µm), confirming that the surface is homogeneously very dark (except in a few localized icy patches, Pommerol et al., 2015; Filacchione et al., 2015).

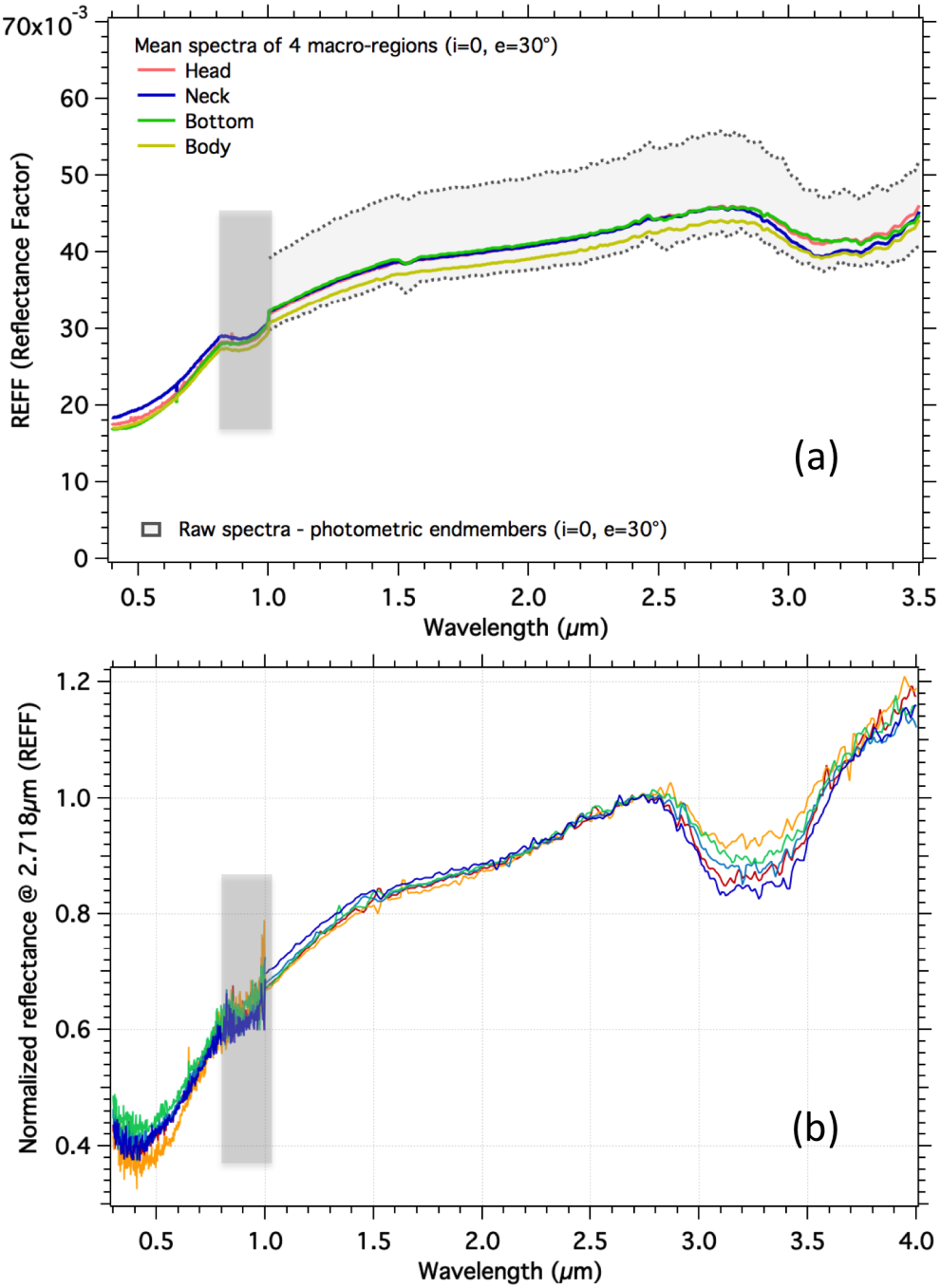


Figure 1: (a): Mean reflectance spectra of four macro-regions as defined by Ciarnello et al. (2015), and two end-members spectra of high and low reflectance. Spectra are given for i=0°, e=g=30°. The feature at 0.95 µm (in dark grey rectangles) is not an absorption band, but an instrumental artifact due to the presence of two bumps: one at 0.9 µm and the other at 1 µm (junction of the two Visible and Infrared channel spectra). Note the slightly higher and bluish reflectance in the neck region, along with the deeper 3.2 µm band. (b) Representative set of REFF spectra normalized to 1 at 2.71 µm. The 3.2 µm band displays variations uncorrelated with the continuum shape.

Infrared spectra normalized at 2.718 µm are very similar from 1 to 2.8 µm across the nucleus (Fig. 1b). On the other hand, the normalized 3.2 µm band depth varies, and does not correlate with the near-infrared slope. These features have therefore distinct carriers. The slope in the visible range displays two main families: a strong red one for most of the regions located in the bottom, body and head, and a low bluish one in the neck. All these features

suggest the presence of at least two different carriers that control the visible slope, the near-infrared slope and the relative depth of the 3.2µm band.

2.3 The 3.2 µm band

The spectral characteristics of the 3.2 µm band and their variations across the nucleus surface were studied on data collected on August 25 (MTP006 STP014 00367589075). Five regions devoid of pixels with shadowed landscape were selected and numbered from 1 to 5 (Fig. 2). Each of them has been related to morphological regions defined by the OSIRIS instrument (Tab. 1; Sierks et al., 2015).

Region	Longitude/Latitude	Region name	Morphology
(1)	34/37	Ma'at	Smooth
(2)	25/19	Ma'at + Hathor	Regolith + Rocky
(3)	53/5	Babi + Aker	Regolith + Rocky
(4)	88/30	Babi + Aten	Regolith + Big depression
(5)	137/45	Ash	Regolith + Big depression

Table 1: Description of the five regions presented in Figure 2. For each the mean longitude and latitude are indicated. Region name and morphology from El-Maarry et al. (2015).

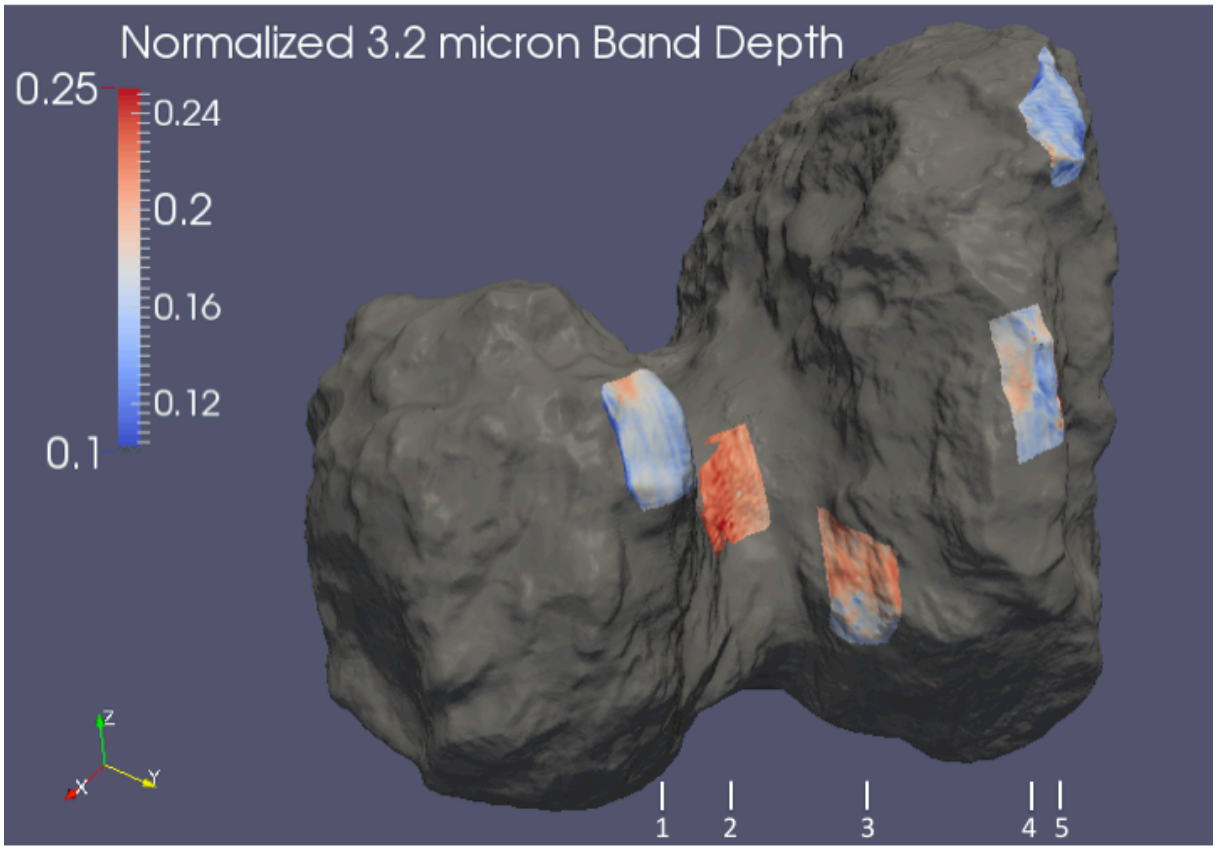


Figure 2: Spatial variations of the depth of the 3.2 µm band in the five regions described in Table 1. Depth is here defined as the intensity of the Gaussian profile that fits the 3.2 µm, after removal of a linear continuum between 3.765 and 2.718 µm.

The 3.2 µm band was extracted from the reflectance spectra (REFF normalized at 2.718 µm) by subtracting a linear continuum between 3.765 and 2.718 µm. Each spectrum was converted into wavenumbers (to get spectral band depth versus photon energy), and fitted with a Gaussian profile:

$$S(\sigma) = Ae^{-(\frac{\sigma-\sigma_0}{FWHM})^2}$$

where σ=1/λ, A is the band depth, *FWHM* the bandwidth and σ_0 is the peak position. These parameters were calculated for each pixel of the five regions, providing averaged values (Tab 2), averaged spectra (Fig. 3) and spatial variations of the spectral parameters (Fig. 2). The statistical distributions of the three parameters were calculated by fitting histograms constructed with the values of each spectral image (Fig. 4). They were fitted with Gaussian profiles, except the band depth of the region 3 that was best fitted with a double Gaussian.

	Region 1	**Region 2**	**Region 3**	**Region 4**	**Region 5**
A	0.17 ± 0.01	0.21 ± 0.01	0.18 ± 0.02	0.16 ± 0.02	0.14 ± 0.01
σ_0 (cm^{-1})	3060 ± 13	3085 ± 8	3075 ± 11	3073 ± 13	3073 ± 26
λ_0 (μm)	3.268 ±0.014	3.241 ± 0.008	3.252 ± 0.011	3.254 ± 0.014	3.254 ± 0.028
FWHM (cm^{-1})	302 ± 16	308 ± 8	306 ± 14	293 ± 12	308 ± 24

Table 2: Mean spectral characteristics of the 3.2 μm band in the five regions showed in Figure 2.

The analysis of the spectral properties of those five regions provides several insights into surface heterogeneity. First, the 3.2 µm band is ubiquitous at the surface of 67P/CG, whatever the morphology and age of the terrains. Second, the band depth varies across the surface, and between the five regions as: (2) (neck) >> (3) > (1) > (4) > (5) (Figs. 2&4; Tab. 2). The band is much deeper in the neck region and, interestingly, the density probability is bimodal in the yellow region that samples both the neck and the body. The correlation between FWHM and σ_0 is less clear, but we observe that the bandwidth is larger and the peak position higher (in wavenumber) in the (neck) region 2. The neck region is known to be the brightest and the bluest and this spectral behavior has been interpreted as a larger abundance of water ice in the surface layers, thanks to shadowing due to local landform (De Sanctis et al., 2015). This region also shows bright spots containing water ice (Pommerol et al., 2015; Fornasier et al., 2015; Fillachione et al., in press). Our spectral analysis does not allow the unambiguous detection of water ice, because its signature merges with that of other broad components. Nevertheless, the spectral evolution between the neck and the body regions is consistent with this interpretation.

Finally two main conclusions emerge from this discussion. *(1)* The 3.2 µm band is present in presumed icy, but also in more refractory terrains. In this respect, most of the carrier of this band is of refractory or semi-volatile nature. *(2)* The 3.2 µm band is present in both fresh deposits and older consolidated morphologies. This last observation points out a limited impact of solar wind irradiation, and will be used below to discuss thoroughly the endogenous versus exogenous nature of this feature.

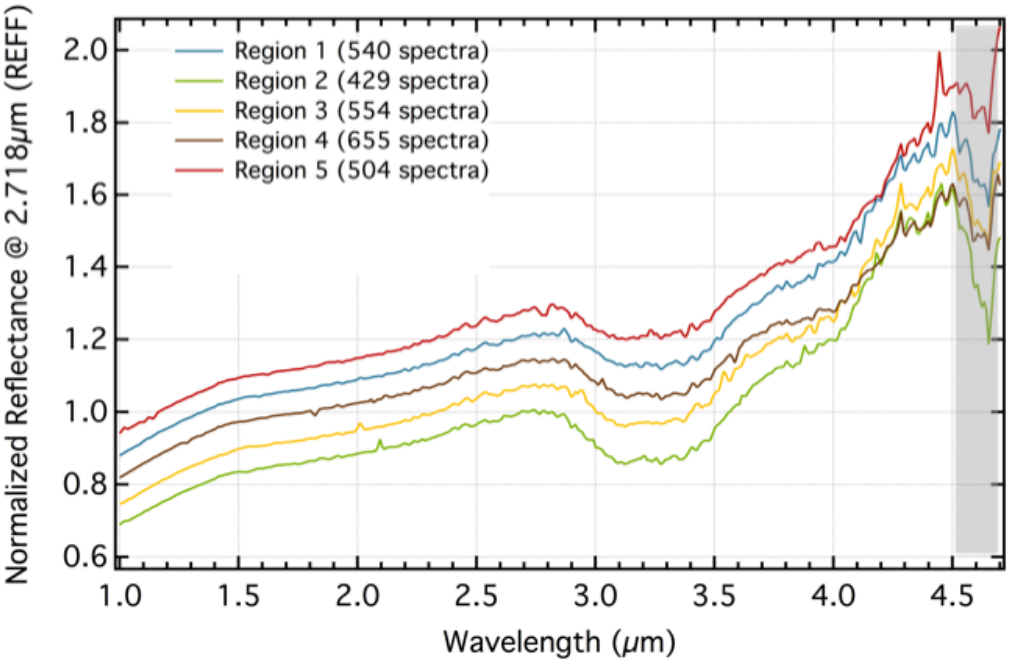


Figure 3: Mean spectra of the five regions depicted in Figure 2 (shifted along vertical axis for clarity). The spectra above 3.7 µm are perturbed by the imperfect thermal correction. The feature centered at ~ 4.6 µm is an artifact induced by the thermal correction.

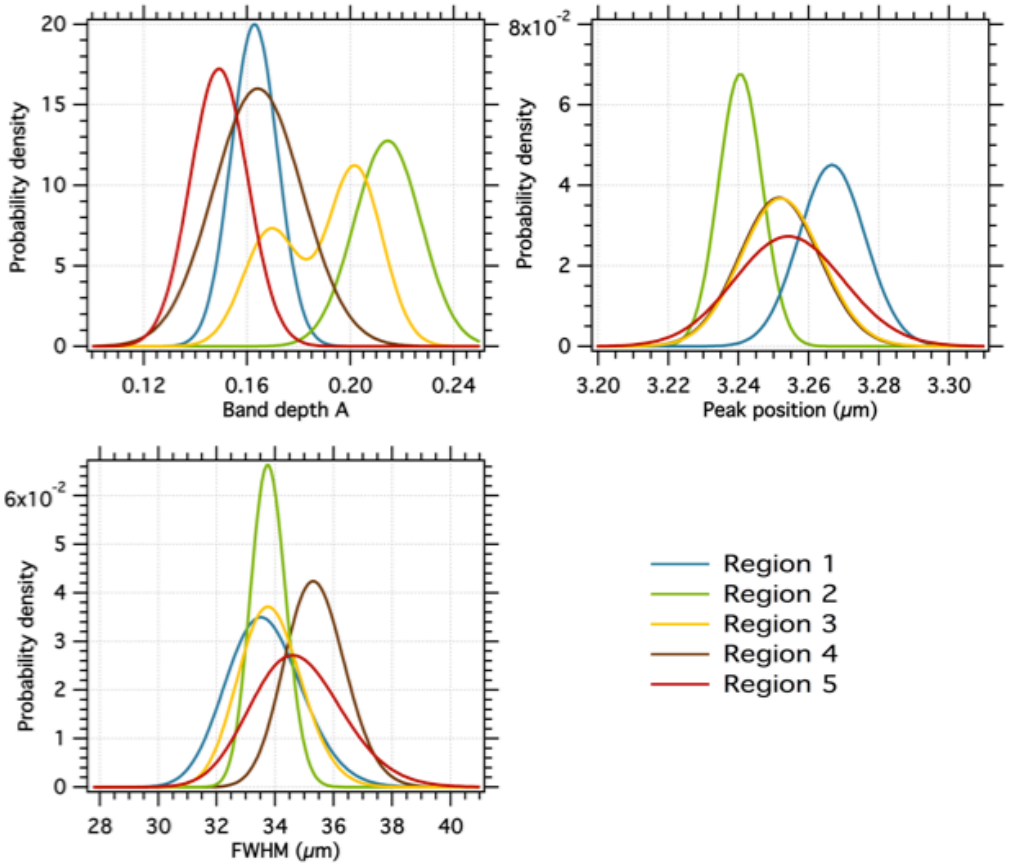


Figure 4: Gaussian fits (probability density) of the spectral parameters distribution of the 3.2 µm band in the five regions.

3. MATERIALS AND METHODS

3.1 Samples

In this study we collected reflectance measurements on *coals, coal tars*, and we have used data collected on *bitumens*, published by Moroz et al. (1998). Firstly, we discuss the relevancy of these materials for simulating a carbon-rich cometary surface.

Coals have been recognized for a long time as potential analogs of meteoritic organics. Berthelot (1868) identified series of alkanes from the hydrogenation of the fresh fall Orgueil (CI) and concluded that a coal-like substance of extraterrestrial origin was present in this chondrite. Since then chemical and structural similarities between coals and meteoritic organics have been extensively described. Organic matter (OM) in primitive meteorites has been operationally described in two distinct components as the soluble organic matter (SOM) that is soluble in usual organic solvents, and the insoluble organic matter (IOM) that is not. SOM can be described as a complex mixture of free molecules (~10^6 different species estimated in Murchison methanol extract, e.g., Schmitt-Kopplin et al. 2010), which does not account for more than 10% of the whole organic content. IOM is a black organic solid that accounts for > 90% of the total organic fraction, and largely controls the optical properties of meteoritic organics (Kerridge, 1999). Chemical composition of IOM in primitive chondrites is fairly similar to that of type III kerogens and coals. Their elemental composition and relative abundances of major chemical groups as methylene and methyl $–CH_2-$ and $–CH_3$, carbonyl C=O and aromatic C=C are fairly similar, and their chemical structures are polyaromatic, with a rather high aromaticity (Gardinier et al., 2000; Alexander et al., 2007; Quirico et al., 2009). In this respect, the mid-IR spectra of chondritic IOM and coals are very similar (Kebukawa et al., 2011; Orthous-Daunay et al., 2013). Nonetheless, the polyaromatic structure of IOM is more cross-linked (e.g. less protonated), and its polyaromatic units may have smaller sizes in average (Remusat et al., 2005; Derenne et al., 2005; Quirico et al., 2009). However, we do not expect a significant effect of these differences on optical properties in both the visible and infrared ranges.

Refractory organic matter in stratospheric IDPs and AMMs of cometary origin shares similarities with chondritic IOM. Raman spectroscopy analyses revealed that those particles also contain a disordered polyaromatic structure (Wopenka, 1998; Quirico et al., 2005; Bonal et al., 2006; Busemann et al., 2009; Starkey et al., 2013; Merouane et al., 2014). Compositional differences have also been reported by micro-IR spectroscopy, X-ray Absorption Near Edge Spectroscopy (XANES) at the C,N,O K-edges and Secondary Ions Mass Spectrometry (SIMS) (Aléon et al., 2001; Flynn et al., 2003; Keller et al., 2004; Matrajt et al., 2005; Merouane et al., 2014). H/C values reported in stratospheric IDPs display a larger range of values than reported in chondritic IOM (Aléon et al., 2001). Aliphatic linkages bridging polyaromatic units in IDPs are less reticulated than in chondritic IOM, and the aliphatic abundance is often lower. Therefore, a large range of H/C ratio was selected for the series of coal samples, and we also used the bitumen series studied by Moroz et al. (1998), which covers a range of elemental composition that encompasses the H/C values reported for stratospheric IDPs.

Finally, a series of six ligno-cellulosic coals from the Penn State Data Bank was selected for this study (http://www.energy.psu.edu/copl/index.html). The series covers a broad range of composition and structure, which is mostly controlled by the extent of thermal history in the sedimentary basin. Each coal is assigned a maturity indicator as the vitrinite reflectance (VR %), which is the mean optical reflectance of vitrinite macerals at 546 nm (Tab. 3). Samples were manually ground in an agate mortar, and the lignite PSOC 1532 was sieved into various size fractions: 560-400, 400-280, 280-200, 200-100, 100-50, 50-25 and < 25 µm. Note that coals are not strictly pure carbonaceous materials, and contain a low

abundance of minerals (Tab. 3). The elemental composition of coal samples, solid bitumens (Moroz et al., 1998), IOM from carbonaceous chondrites (Alexander et al., 2007) and the H/C ratio measured in stratospheric IDPs are displayed in Figure 5. The composition of analogs encompasses fairly that of cosmomaterial. Finally, a coal tar spectrum from Cloutis et al. (2013) was found to fit well the spectra of 67P/CG. Therefore, we studied two coal tars produced from the pyrolysis of oxygen-poor bituminous coals (Table 3).

Three carbonaceous chondrites were used for comparison with 67P/CG spectra: Orgueil (CI), Murchison (CM) and GRO 95577 (CR), in order to sample the three main chemical classes of primitive carbonaceous chondrites. These chondrites did not experience thermal metamorphism in their parent body and are considered primitive objects. Samples were also ground in an agate mortar. Other classes of carbonaceous chondrites (CO, CV, CK) were not considered as they experienced intensive thermal metamorphism in their parent body. The factors controlling the reflectance spectra of CI, CM and CR carbonaceous chondrites have been investigating by Garenne et al., (2015). Grain size was not found as a critical parameter, while the chondrule/matrix ratio may have a significant effect.

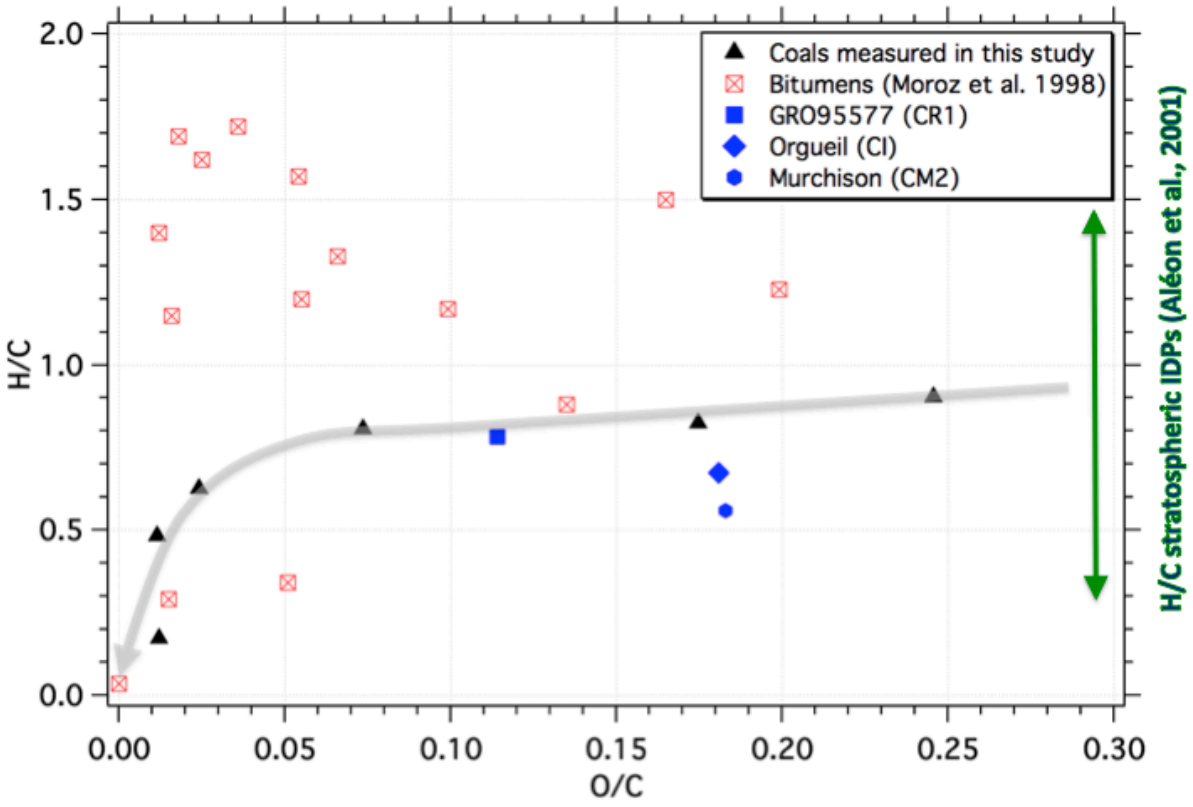


Figure 5: H/C vs. O/C diagram of coal samples used in this study (provided by Penn State University Data Bank), of bitumens studied in Moroz et al. (1998) and of Insoluble Organic Matter extracted from 3 primitive carbonaceous chondrites (Alexander et al., 2007). The grey arrow draws the thermal evolution of the coal samples, from lignite to anthracite.

3.2 Experimental techniques

Reflectance measurements were collected with a spectro-gonio-radiometer designed and built at IPAG (Brissaud et al., 2004). This instrument operated over the spectral range 0.4-4.8 µm with a spectral sampling of 20 nm, and a spectral resolution varying from 5 to 40 nm. The measurements were collected at normal incidence (i=0°) and emergence e=30°

within the incidence plane (g=30°). These measurements were unaffected by the narrow opposition effect that is present only a few degrees around opposition geometry. The reflectance factor was calculated as the ratio of the sample radiance $I_{\text{sample}}(i,e,\lambda)$ divided by the radiance of commercial diffuse reflectance reference surfaces $I_{\text{reference}}(i,e,\lambda)$ from Labsphere company (Spectralon SR-99 for 0.4-2.5 µm; Infragold, for 2.5-4.8 µm) and multiplied by the calibrated reflectance factor of the reference surface (Bonnefoy, 2001):

$$REFF(i,e,\lambda) = \frac{I_{sample}(\mathrm{i,e,\lambda})}{I_{reference}(\mathrm{i,e,\lambda})} REFF_{REF}(i,e,\lambda)$$

Measurements were run under ambient atmosphere for coals and coal tars, and within an environmental cell for carbonaceous chondrites. This cell allowed the removal of the signature of terrestrial adsorbed water, as the sample was placed under secondary vacuum ($<10^{-5}$ mbar) at 80°C during at least one hour. The elemental compositions H/C and O/C of the coal tars CT1 and CT2 were measured at Laboratoire Génie des Procédés et des Matériaux (Ecole Centrale de Paris) with a CE Instruments NC 2500 series elemental analyzer linked to a gas chromatographic column. Raman spectra were collected at Laboratoire de Sciences de la Terre with a Horiba LabRam spectrometer coupled with a microscope equipped with a x100 objective, leading to a circular spot with a 1-2 µm diameter. We used a 600 gr/mm grating and a 514 nm radiation delivered by an Ar+ Spectra Physics laser. The power on the sample was ~ 50 µW. Coal tar samples were found very sensitive to laser irradiation, therefore we used a very low laser power.

	H/C	O/C	VR (%)	Moisture	Ash (wt%)
PSOC 1532	0.90	0.25	0.33	25.76	9.46
DECS 09	0.82	0.17	0.38	39.35	6.37
DECS 15	0.81	0.07	0.8	3.15	10.13
PSOC 1521	0.63	0.02	1.61	5.29	11.16
PSOC 379	0.48	0.01	2.8	4.92	16.06
PSOC 1468	0.17	0.01	5.45	5.92	6.83
CT1	0.57	1.09	---	---	
CT2	0.55	1.78	---	---	
Orgueil (IOM)	0.67	0.18	---	---	
Murchison (IOM)	0.59	0.18	---	---	
GRO 95577 (IOM)	0.79	0.11	---	---	

Table 3: H/C and O/C elemental composition of the samples studied. For the coals from Penn State Data Bank, the vitrinite reflectance (i.e. maturity), moisture abundance and ash content are indicated. Elemental compositions measured at Ecole Centrale de Paris for the coal tars CT1 and CT2 (courtesy of A. Buch), and by Alexander et al. (2007) for the IOM of the three chondrites.

4. LABORATORY MEASUREMENTS

4.1 Coals

Reflectance spectra of coals (ground but not sieved) are reported in Figure 6. All spectra have a low reflectance in the visible range, consistent with the vitrinite reflectance values provided by the Penn State Data Bank (Tab. 3). They cover a broad range of photometric variations in the near infrared between 1 and 2.7 µm. PSOC 1532 and DECS 09 have the highest NIR reflectance (REFF ~ 0.35-0.45) that peaks at ~ 2.2 µm. The NIR reflectance level decreases upon increasing coal maturity, and the most mature coal – the anthracite PSOC 1468 - shows a very flat and low reflectance factor at ~0.05 over the whole visible and infrared ranges. The band at 2.3 µm is assigned to overtone/combination of the stretching modes of methylene (CH_2) and methyl (CH_3) chemical groups. The band at ~2.5 µm may be due to a combination of C-H stretch with C-C stretch. They are observed in the spectra of the less mature coals, but not in the other in agreement with alkyl loss during late diagenesis and catagenesis. The feature centered at 1.9 µm (yellow ribbon in Fig. 6) is due to molecular water adsorbed on the samples or interlayer water in clays, as measurements were not collected under a controlled atmosphere. The strength of this band is in good agreement with moisture measurements provided by Penn State Data Bank (Tab. 3). The sharp drop at ~2.7 µm, which appears as a narrow band (e.g. in PSOC 379), is assigned to the OH stretching of structural hydroxyl in clays.

Above 2.7 µm, the reflectance spectra display different absorptions: (i) molecular water, mostly due to moisture, that results in a broad band at ~ 3.1 µm whose strength decreases with maturity; (ii) a band due to aromatic C-H at 3.28 µm. The strength of the aromatic C-H band increases upon increasing maturity; (iii) a band centered at ~ 3.44 µm, with a substructure whose shape is controlled by the symmetric and antisymmetric stretching vibration modes of the CH_2 and CH_3 chemical groups.

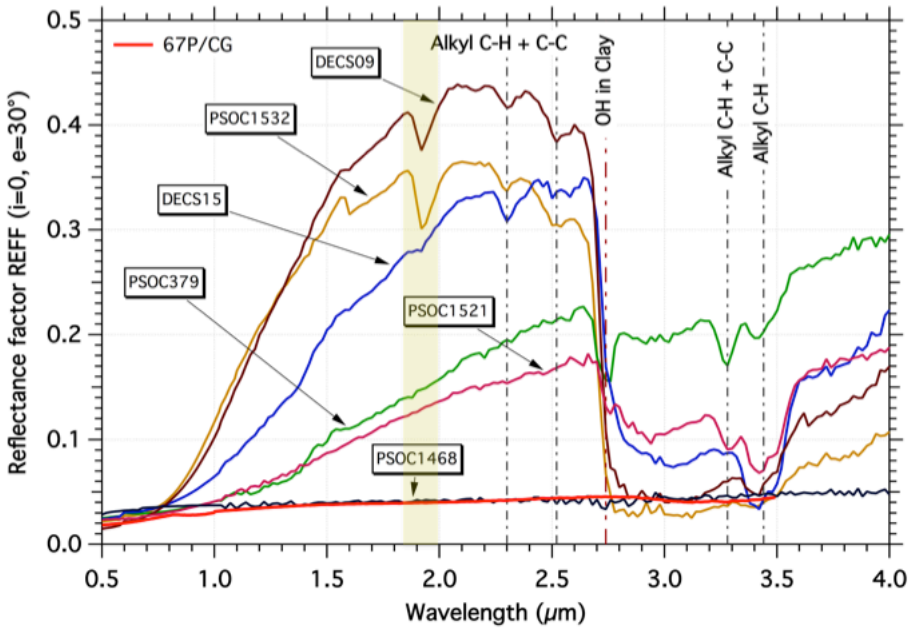


Figure 6: REFF spectra of ground coals of different maturities. Spectra were collected under ambient atmosphere. The yellow ribbon points to the presence of adsorbed water on the samples. The red mixed line points to the OH vibration in clays. VR: vitrinite reflectance. Grey mixed lines indicate the position of the alkyl and aromatic C-H vibrations (3.44 and 3.28 μm, respectively), an overtone/combination of alkyl and C-C vibrations at 2.3 and 2.52 μm.

Spectra of PSOC 1532 have been collected for different grain size fractions (Fig. 7). There is little or negligible effect of grain size on the visible reflectance, but a very significant effect in the range 1-2.7 µm. The maximum reflectance (at ~ 1.9 µm) varies greatly with grain size, and increases upon decreasing grain size. Even for the larger grain sizes, the reflectance at 2.2 µm does not drop below 0.08. A similar spectral behavior as a function of particle size has earlier been reported by Moroz et al. (1998) for asphaltite separates.

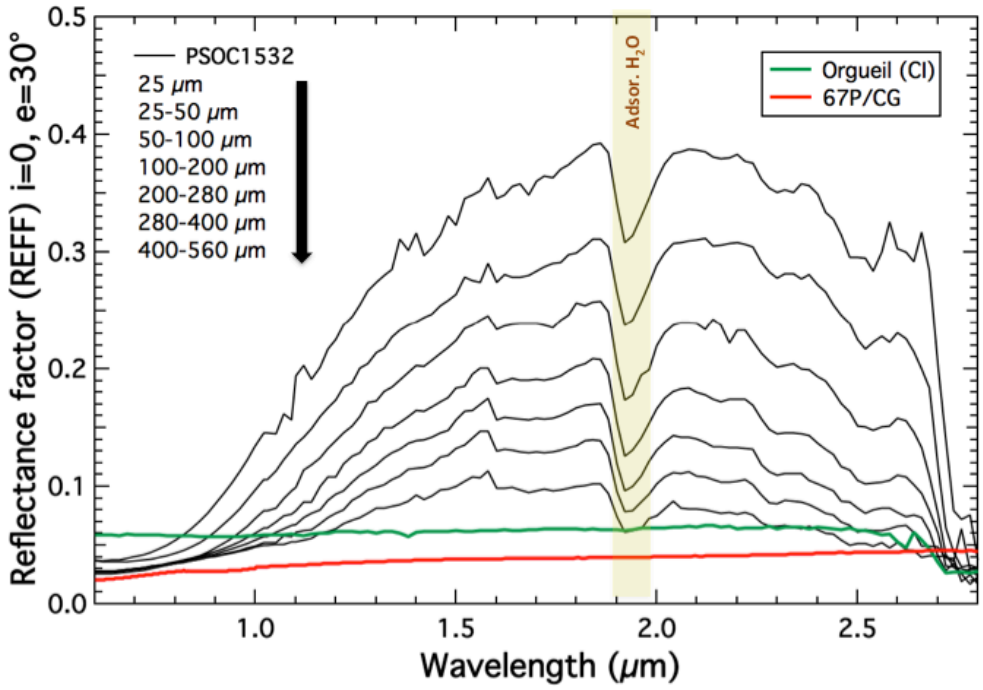


Figure 7: Reflectance factor of coal PSOC1532 collected for various grain size ranges. The maximum reflectance factor decreases upon increasing grain size in the near-infrared range, while the reflectance in the visible remains at values below 0.04. The reflectance factors of 67P/CG and Orgueil chondrite are plotted for comparison. The yellow ribbon points to the presence of adsorbed water on the samples.

4.2 Coal tars

The spectra of coal tar samples CT1 and CT2 (grain size < 50 µm) are similar to each other and resemble that of the anthracite coal PSOC 1468 (Fig. 8). They are dark both in the visible and in the near-infrared, and also show a steep reddish slope in the visible, in agreement with the coal tar measurements of Cloutis et al. (1994). A deep 3.28 µm feature is present, along with a weak alkyl band at 3.44 µm. CT1 and CT2 are aromatic-rich samples, and the strong absorption throughout the infrared range points to the presence of large polycyclic aromatic species. Coal tars are however chemically and structurally dissimilar to anthracite. The respective Raman spectra (514 nm excitation) of CT1 and coal PSOC 1468 (Fig. 9) appear significantly different, though their reflectance spectra are rather similar (Fig. 8). The Raman spectrum of CT1 consists in a fluorescence background onto which the so-called G and D bands are superimposed. These G and D bands are usually used to determine the degree of structural order of carbonaceous materials, with D pointing to disorder (Ferrari and Robertson, 2001). Here they are rather broad, and in this respect this spectrum resembles that of immature coals. In contrast, the spectrum of PSOC 1468 is devoid of fluorescence and show narrow G and D bands, consistent with the high maturity. Two different carbonaceous materials thus give rise to almost similar reflectance spectra.

In fact, the coal tar samples contain a large fraction of soluble molecules. The shape and broadness of the G and D bands are controlled by the size of free Polycyclic Aromatic

Hydrocarbons (PAHs) (Castiglioni et al., 2001). Based on these parameters, our Raman data are consistent with a dominant population of small PAHs. However, our coal tar samples also contain larger PAHs that account for the strong electronic absorption in the near-infrared range. Finally, coal tars are less refractory than coals, chondritic IOM and refractory organics in IDPs and AMMs, and the size distribution of their aromatic species is much broader, encompassing very small to large PAHs. Note that the poor resistance to thermal stress under laser irradiation observed during Raman measurements fully supports this view.

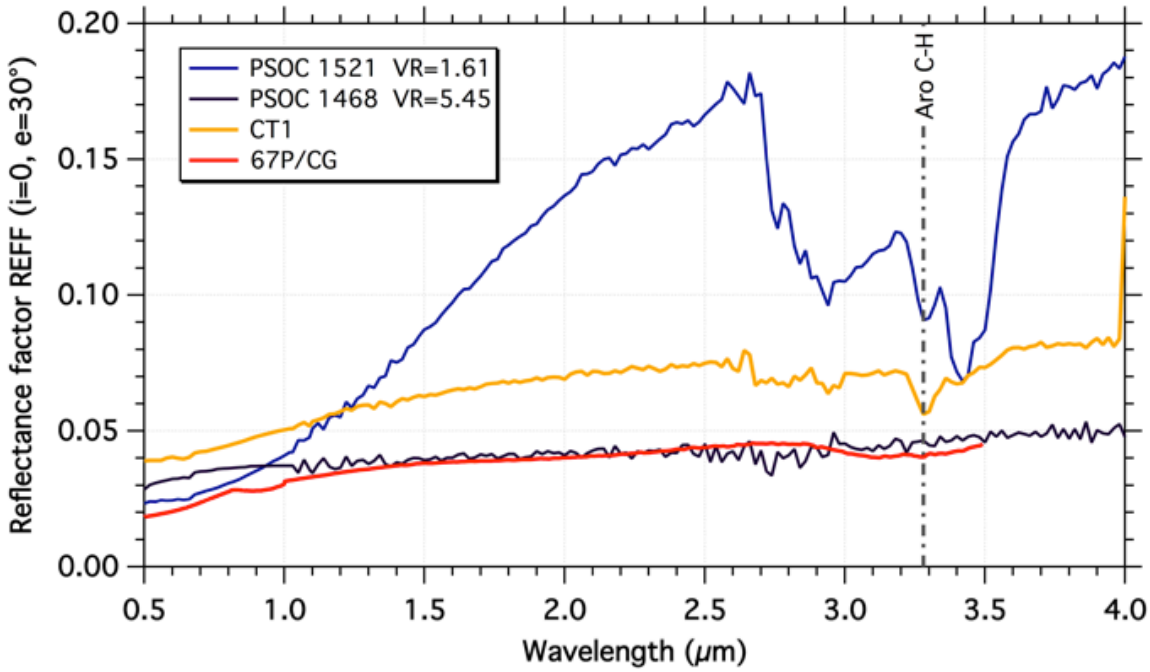


Figure 8: The spectrum of the coal tar CT1 plotted along with the spectra of coals PSOC 1521 and PSOC 1468. The band centered at ~3 µm results from the combination of moisture, hydroxyl in clays and possibly organic OH groups.

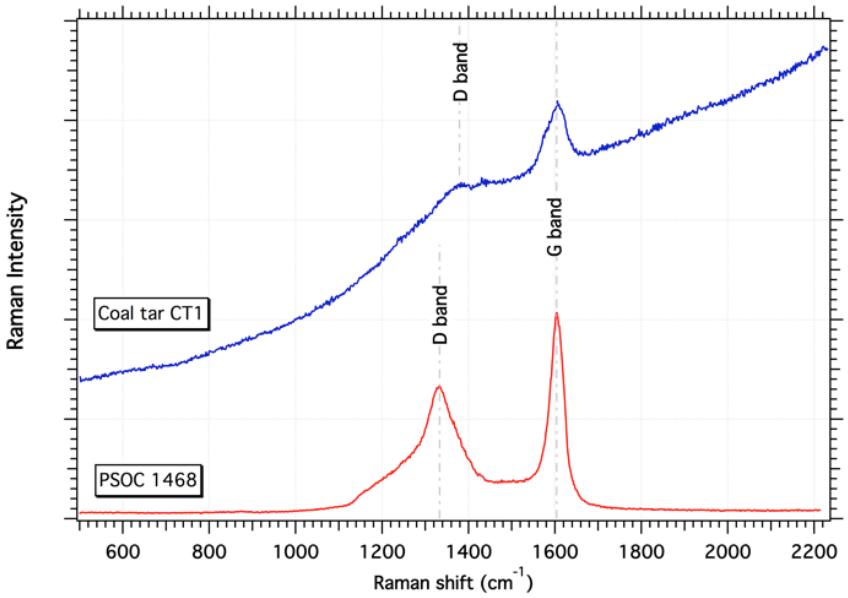


Figure 9: Raman spectra of coal tar CT1 and anthracite PSOC 1468. Spectra recorded with a 514 nm wavelength excitation.

4.3 Carbonaceous chondrites

The reflectance spectra of the three powders of carbonaceous chondrites Orgueil (CI), Murchison (CM) and GRO 95577 (CR1) are displayed in Figure 10 (see Garenne et al., 2015 for extensive details on measurements). The reflectance spectra are dark in the visible and the infrared ranges (0.4-4 µm). Below 2.5 µm, the spectrum of Orgueil is flat, that of Murchison has a weak broad absorption feature centered at ~ 0.9 µm, while that of GRO 95577 is flat in the visible, but has a slight reddish slope in the near-infrared. The (slight) differences in the reflectance level between the three samples are consistent with their modal abundances of chondrules that increase from Orgueil to GRO95577. The spectra all show a broad absorption band centered around 2.7-2.9 µm that is due to structural OH trapped in serpentine or smectite (Orgueil), with some contribution from chemically bound (smectite) and/or physisorbed water at longer wavelengths. The position of this band is controlled by the Mg/Fe ratio in phyllosilicates (Beck et al., 2010; Garenne et al., 2015).

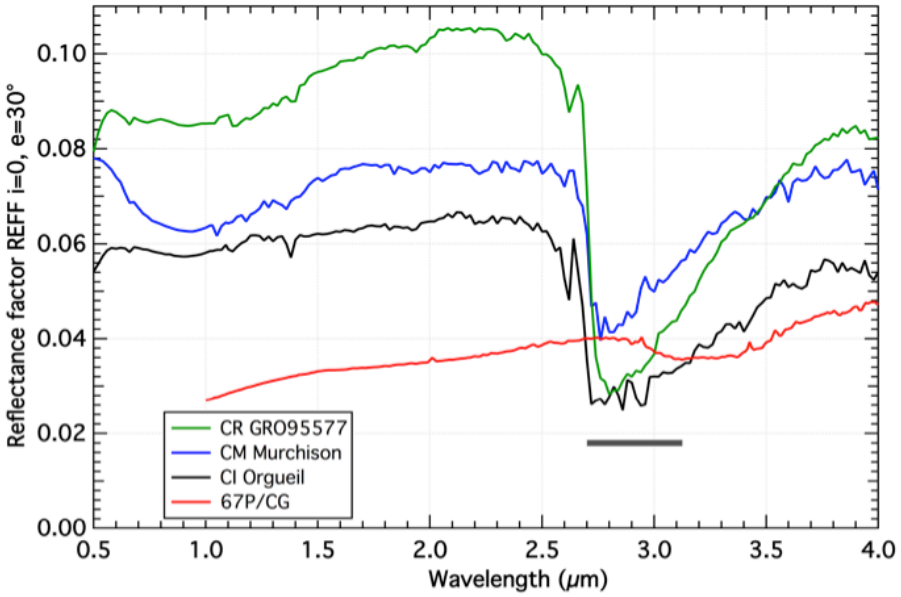


Figure 10: Reflectance spectra of ground Orgueil, Murchison and GRO 95577 chondrites, plotted along with the spectrum of 67P/CG.

5. DISCUSSION

5.1 Spectral reflectance properties of cometary analogs

As discussed in section 4.1, the reflectance spectra of coal samples display variations that are controlled at first order by maturity (rated by the vitrinite reflectance) (Fig. 6). Coal darkness is physically related to the electronic gap E_g, which is itself controlled to a large extent by the size of the aromatic units composing the polyaromatic structure ($E_g \sim 6M^{-0.5}$, M number of rings; Robertson, 1995). As maturity increases, the size of the aromatic units increases and E_g decreases, resulting in a stronger visible absorption and the extension of absorption towards lower energy in the near-infrared. In this respect, as any carbonization process is accompanied by the condensation of aromatic units, the spectral behavior of this series of coals is consistent with that of any series of carbonaceous materials produced from a thermal process, either in natural or artificial conditions. A similar trend was observed for a series of natural bitumens spanning a broader range of elemental compositions and chemical structures (Moroz et al., 1998). As for coals, bitumen maturity (as rated by H/C and carbon aromaticity) was found to control the reflectance spectra, in a way similar to coals (Fig. 11).

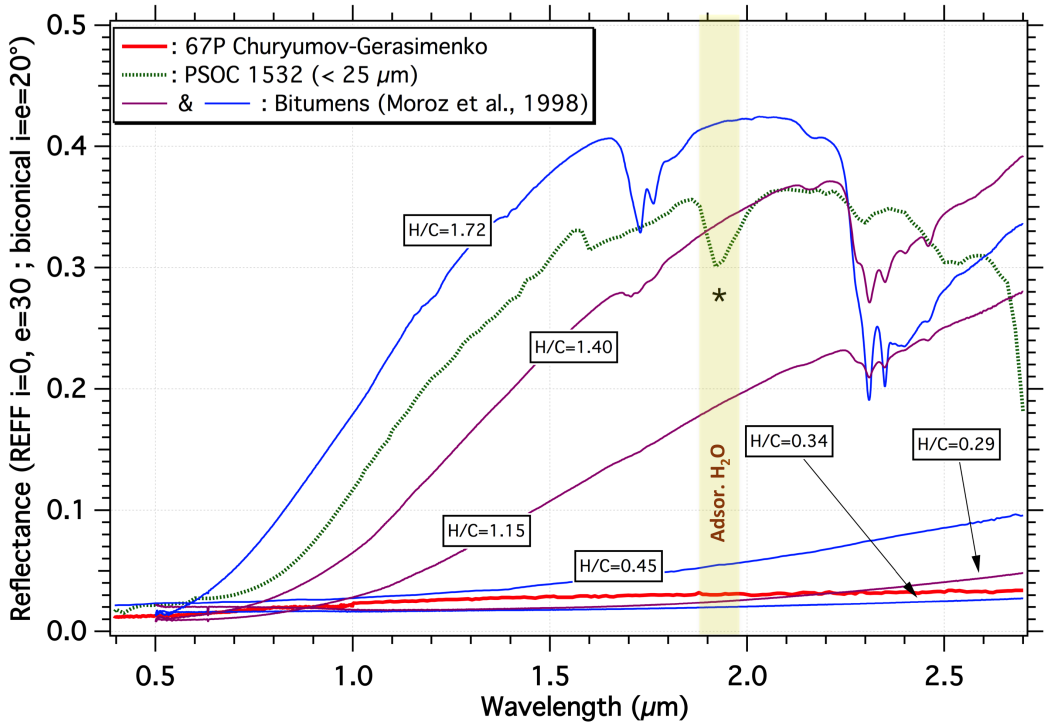


Figure 11: Reflectance spectra of bitumen samples (<25 µm) from Moroz et al. (1998) plotted along with spectra of coal PSOC 1532 and 67P/CG. The yellow ribbon points to the presence of adsorbed water in the coal sample.

Along with generally similar optical trends, described above, there are some near-infrared spectral differences between coals and solid oil bitumens, which are caused by their dissimilarities in composition and chemical structures. Bitumen spectra do not show NIR features caused by high moisture content and mineral impurities typical of immature (low rank) coals (Fig. 11). Compared to coals with similar (H+O+N+S)/C ratios, solid oil bitumens are characterized by a lower degree of carbon aromaticity and are depleted in oxygen functionalities. As a result, red bitumens show pronounced aliphatic absorption bands near 1.7, 2.3 and 3.4 μm, while in the spectra of coals such features are much weaker or absent (Figs. 6, 11). Reflectance spectra of solid oil bitumen samples shown in Fig. 11 were measured at somewhat different geometry (i=e=20°; biconical reflectance) than the samples from this study (i=0°; e=30°; bidirectional reflectance). However, interlaboratory

comparisons showed negligible differences between biconical measurements performed at i=e=20° and bidirectional measurements at i=0°; e=30°. Therefore, we do not expect significant spectral discrepancies, introduced by viewing geometry, between the spectra shown in Fig. 11.

Coal tar samples appear as fair *optical analogs* of comet 67P/CG (Fig. 8). They have low albedo in the visible and in the near-infrared ranges, and their Raman spectra point to a disordered polyaromatic material, as observed in interplanetary dusts (Fig. 9). However, they are not relevant *chemical analogs*, i.e. their composition and their structure are dissimilar with those of cometary refractory organics. Indeed, coal tars are described as a mixture of free molecules with a highly aromatic character, and are chemically distinct from chondritic IOM (e.g. Remusat et al., 2005, Flynn et al., 2003; Matrajt et al., 2005; Merouane et al., 2014).

5.2 Dark organics and opaque minerals in 67P/CG

In this subsection we restrict the discussion to the wavelength range 0.4-2.5 µm. Figures 6,7,8 and 10 display the reflectance factor REFF of 67P/CG, coals and primitive chondrites collected under similar observational geometries (i=0, e=30°). The bulk abundance of organic matter in Orgueil is ~ 4wt%, mostly in the form of IOM (> 70%). Among the coals studied here, DECS09 and PSOC 1532 are the samples that most resemble Orgueil IOM. Hence, they have close elemental composition, close relative abundances of CH_2/CH_3, carbonyl and aromatic C=C groups, and they have a very disordered polyaromatic structure.

The reflectance spectra of both these coal samples do not match that of the bulk Orgueil chondrite, whatever their grain size distribution. In particular, Orgueil is slightly brighter in the visible range, and above 0.8 µm DECS09 and PSOC 1532 are much brighter, reaching a reflectance factor of ~ 0.4-0.5 at 2 µm (for the < 25 µm fraction; Fig. 7). In contrast, the spectrum of Orgueil is flat in the range 0.4-2.5 µm with a reflectance value of ~0.06. The higher reflectance in the visible is presumably due to refractory carbon abundance, along with the presence of bright minerals, e.g. sulfates that result from the oxidation of unstable sulfides under terrestrial atmosphere and that are widespread in Orgueil (Gounelle and Zolensky, 2001). In the infrared range, IOM reflectance (as inferred from those of DECS09/PSOC 1532) does not account for the very low reflectance of bulk Orgueil, and we infer the spectral contribution of opaque minerals as sulfides (mostly pyrrhotite and troilite) and oxides (magnetite). Fe-Ni alloys (as either kamacite or taenite) are poorly abundant in Orgueil, so we do not expect their significant contribution. Similar observations are reported for the CM chondrite Murchison (reflectance ~0.07, with a broad and moderate absorption at 0.9 µm) and the CR chondrite GRO 95577 (slightly increasing reflectance from 0.85 to 0.11). As reported in the section 4.3, the reflectance level is slightly higher for Murchison and for GRO 95577 with respect to the other two meteorites. The modal abundance of chondrules within these 3 chondrites varies from ~ 0% (Orgueil), to ~20% (Murchison) up to ~50% (GRO 95577), which is consistent with this reflectance trend. The reason is that olivine and pyroxenes from chondrules are not dark and increase the reflectance level.

67P/CG is characterized by very low reflectance, reddish slope in the visible and weak slope in the near-infrared (Fig. 1). Among our samples, best spectral matches are obtained with the anthracite PSOC1468 and to a lesser extent with the coal tars. The most mature (carbonized) members of the solid oil bitumen series from Moroz et al. (1998) (high and medium anthraxolites) also spectrally resemble the 67P/CG surface in the visible and near-infrared. Though providing a good optical fit, anthracite is definitely not a plausible analogue for cometary refractory organics. This very mature coal (VR=5.45 %) experienced a high temperature heating at 200-300 °C over a long duration (~ 0.1-1 Myr). It lost a large fraction of its H and O heteroatoms, and contains large aromatic units that are definitely inconsistent

with the very small units present in refractory carbonaceous materials of cometary grains. Mature carbonaceous materials in stratospheric IDPs are very unusual, and generally attributed to an asteroidal origin (Wopenka, 1988; Bonal et al., 2006; 2011; Busemann et al., 2009). Similar conclusions should be drawn for anthraxolites, as well as for coal tars. Coal tars are complex mixtures of hydrogenated carbon with a large aromatic component, including very large aromatic units accordingly to the pyrolytic conditions under which they were produced. As discussed before, they should be described as a complex mix of soluble species with a strong aromatic character, at odd with the composition of refractory organics from stratospheric IDPs, which generally have a significant alkyl component and contain oxygenated chemical groups (Flynn et al., 2003; Keller et al., 2004; Matrajt et al., 2005; Merouane et al., 2014).

More suitable analogs (in terms of structure and chemical composition) are less mature coals and solid oil bitumens, whose compositions encompass those of stratospheric IDPs. In reflectance spectra of 67P/CG we do not observe the overtone and combination modes of CH_2 and CH_3 groups (near 1.7 and 2.3 µm), while they are observed in asphaltites and kerites, and to a lesser extent in immature coals (Fig. 6, 11). The strength of the band in the near-infrared spectra of pure bitumens and coals correlates with the H/C ratio. The lack of detection of these bands in 67P/CG spectra may be due to a low H/C ratio in the surface organic material or a low content of organics, but can also be due to the faintness of the band with respect to the signal-to-noise ratio, as a consequence of the low reflectance. Finally, these weak bands can be completely suppressed in the spectra due to the presence of an absorbing material. This lack of detection is consistent with the apparent weakness of the broad 3.2 µm band, which could host vibration modes of C-H chemical groups (see discussion below). Last, the low visible reflectance in 67P/CG, with respect to chondrites, strongly suggests a higher abundance of refractory organics at the surface of the comet. This result is fully consistent with the higher abundance of these organics in stratospheric IDPs (15 wt% in average, against 4-5 wt%; Thomas et al., 1993). However, the high reflectance factor of immature coals and bitumens is at odd with the low reflectance factor of 67P/CG in the near infrared range (Fig. 6, 11). This leads to the conclusion that refractory organic matter alone cannot account for the low reflectance in the near-infrared range, and that other components absorb within this spectral range.

The nature of those phases cannot be identified from VIRTIS spectra, but it can be inferred from the composition of cometary grains analyzed in the laboratory. As reported before, there is no unequivocal information carried in the spectra, and we need inputs from other sources. So far, instruments aboard the Rosetta mission dedicated to the characterization of dust – COSIMA, MIDAS, GIADA - have provided insightful information on flux, velocities and textures, but not yet on composition. In contrast, systematic mineralogical characterization of Antarctic micrometeorites, stratospheric IDPs and Wild 2 grains thoroughly determine the nature and compositions of mineral phases. Sulfides are an abundant component of those grains. Their composition in AMMs is close to troilite (FeS), while pentlandite that is widespread in some primitive carbonaceous chondrites is very scarce (Dobrica et al., 2009). Sulfides have also been detected as abundant minerals in STARDUST grains sampled from the Wild2 comet (Zolensky et al. 2006; Leroux et al., 2008). Their composition was basically devoid of Ni, but the Fe/S could not be determined accurately due to heating artifacts triggered by the slowing down in aerogel collectors. There is no systematic report of Fe-Ni alloys in AMMs, but they have been reported in stratospheric IDPs and STARDUST grains (Rietmeijer, 1998; Ogliore et al., 2010). However, in the STARDUST samples, such metallic grains could be formed due to the preferential loss of S during the capture. The mineralogy of cometary grains is basically anhydrous, in this respect we do not

expect indigenous oxides or oxihydroxides (e.g. magnetite, ferrihydrite) and opaque minerals are basically limited to anhydrous sulfides and Fe-Ni alloys.

Optical constants of Fe and Ni metal available in literature reveal that the imaginary part of the refractory index (k) continuously increases from 0.4 up to 5 µm, varying from ~ 2 to 12 (Lynch et al., 1971; Weaver et al., 1979; Ordal et al., 1983). From these data we infer that kamacite and taenite alloys are strongly absorbing through the visible and infrared, and, if present, should certainly significantly contribute to 67P/CG darkness. Optical properties of sulfides depend on composition and structure (Bither et al., 1969). Pyrite (FeS_2) is weakly absorbing in the near-infrared. Unfortunately, no optical constants are available for troilite (FeS) and pyrrhotite ($Fe_{1-x}S$) at wavelengths longer than 1 µm. Reflectance measurements of Britt et al. (1992) show that reflectance of troilite in the range 0.4-2.7 µm decreases with decreasing grain size. This spectral behavior is consistent with absorbing grains throughout this wavelength range, and we infer that, unlike pyrite, troilite is most likely opaque in the range 0.4-2.7 µm.

5.3 The 3.2 µm band

The broad 3.2 µm band, extending from ~2.9 to 3.7 µm, appears in all spectra of 67P/CG. Plausible candidates are –OH, $-CH_2/CH_3$ and $–NH/NH_2$ chemical groups, as well as aromatic C-H and ions as NH_4^+ (Lien-Vien et al., 1991). Below we examine the relevant possible carriers of those chemical groups or ions. Note that our discussion does not include isolated surface patches that contain water ice, which broadens and shifts the band towards shorter wavelengths (De Sanctis et al., 2015; Filacchione et al., 2015).

5.3.1 C-H vibrations in aliphatic and aromatic hydrocarbons

C-H bonds in methylene (CH_2)-, methyl (CH_3)-groups and in aromatic structures have symmetric and antisymmetric stretching vibration modes in this spectral region. These features appear clearly in the spectra of bitumens, and of an aliphatic-rich tholin (Fig.12; Quirico et al., 2008). They form a broad complex absorption feature between 3.3 and 3.6 µm. Stretching vibrations of CH_2 and CH_3 groups give rise to four overlapping bands centered near 3.37-3.39, 3.4 and 3.5 µm. In reflectance spectra of asphaltite, wurzilite and low kerite bitumens, the bands are not well resolved due to saturation (Fig. 11; Moroz et al. 1998). C-H stretches in aromatic structures give rise to a complex absorption feature centered between 3.27 and 3.3 µm. The latter feature is well pronounced in high kerites, medium- and low anthraxolites (Fig. 12; Moroz et al., 1998) and relatively mature coals (Fig. 6; De Bergh et al., 2008).

The C-H bands may contribute to the 3.2 µm band regarding band positions, but the individual bands due to the respective vibration modes are not resolved in the spectra of 67P/CG. This lack of detection may be either due to the low signal-to-noise ratio, or due to the overlapping with several vibration modes from other chemical groups. At present, there is no firm identification of specific aliphatic and/or aromatic functional groups in reflectance spectra of 67P/CG.

5.3.2 Amine groups

NH and NH_2 chemical groups (secondary and primary amines, respectively) have typical symmetric and antisymmetric vibration modes within the spectral region of the 3.2 µm band. Fig. 12 shows a comparison of a 67P/CG reflectance spectrum with transmittance spectra of two tholins and an HCN polymer (Quirico et al., 2008). The amine band extends from 2.7 to 3.7 µm, and is broader than the 3.2 µm band towards shorter wavelengths. The substructure with peaks at ~ 3.00 and 3.12 µm does not appear in 67P/CG spectrum, and the

band is centered at ~3.0 µm. Obviously, NH/NH_2 groups cannot be the unique carriers of the 3.2 µm band, and their significant contribution to this feature is unlikely. Moreover, significant contribution of N-rich functional groups is challenged in the light of cosmochemical data. Nitrogen abundance in cometary grains is known to be low in general, and amine groups have not been detected through FTIR microscopy on stratospheric IDPs (e.g. Flynn et al., 2003; Matrajt et al., 2005; Merouane et al., 2014). N-rich particles, like UltraCarbonaceous Antarctic micrometeorites (UCAMMs), are not representative of the mainstream of dust population (Dobrica et al., 2011; Dartois et al., 2013).

5.3.3 Hydroxyl group

The OH group can be present in both inorganic and organic forms. A first type of possible carriers could be hydroxylated minerals: phyllosilicates, oxyhydroxides, or OH-bearing sulfides. Comparison with carbonaceous chondrites shows that OH in Mg-Fe serpentines, which are the major hydrated minerals in these meteorites, give rise to an absorption band centered between 2.7 and 2.9 µm (Fig. 10). This band is assigned to the stretching vibration of structural OH groups. Its wavelength position is controlled by the Fe/Mg ratio, but does not extend above 2.9 µm (Beck et al., 2010). In this respect, its contribution to the 3.2 µm band is not significant. Similar conclusions should be drawn for oxyhydroxide minerals, as ferrihydrite and goethite, whose main band controlled by OH stretching peaks at ~ 3.1 µm and ~2.9 µm, respectively (Lair et al., 2006; Beck et al., 2011). Another OH-bearing mineral abundant in some carbonaceous chondrites (CM-chondrites) is an OH-bearing Fe-sulfide tochilinite. Its reflectance spectra show absorption bands (Moroz et al., 2006), whose positions (2.7-2.9 µm) and shapes make tochilinite an unlikely contributor to the 3.2-µm band of 67/CG. Note that the presence of hydroxylated minerals relies on extensive aqueous circulation in the parent body, which is at odd with systematic mineralogical analysis of stratospheric IDPs and Antarctic micrometeorites. This issue is addressed in detail below.

The OH group can also be present in an organic form in either alcohols or carboxylic acids (Lin-Vien et al., 1991). Alcoholic hydroxyl generally results as a band extending from 2.7 to 3.2 µm, which does not encompass the broadness of the 3.2 band. The band of carboxylic acids spans a much broader spectral region and may account for a large part of the 3.2 µm band. This broadness is due to the ability of the COOH group to establish hydrogen bonds, and in this respect is controlled by the COOH concentration. The carrier of COOH and OH groups might be molecules that have a molecular weight consistent with their thermodynamic stability in the first tens of micrometer of 67P/CG surface. In this respect, they may share similarities with soluble organic matter in primitive meteorites, which is dominated by carboxylic/dicarboxylic acids (Sephton, 2002). They also could be present as part of the macromolecular structure of the polyaromatic solid that possibly controls the low reflectance of comet 67P/CG in the visible range. However the depth of the 3.2 µm band displays variations across the nucleus that are not correlated with the visible and near-infrared slopes in normalized spectra (Fig. 1). Furthermore, COOH as a chemical group branched in a polyaromatic solid skeleton has likely limited interactions with other COOH groups, or with any group with which hydrogen bonds could be established. In this respect, the spectral contribution of COOH groups over the full broadness of the 3.2 µm band appears more consistent with a complex mixture of free low molecular weight molecules and not with chemical groups inserted in the macromolecular network of a dark polyaromatic solid. This kind of mixture is less volatile than ices, and is named hereafter *semi-volatile*.

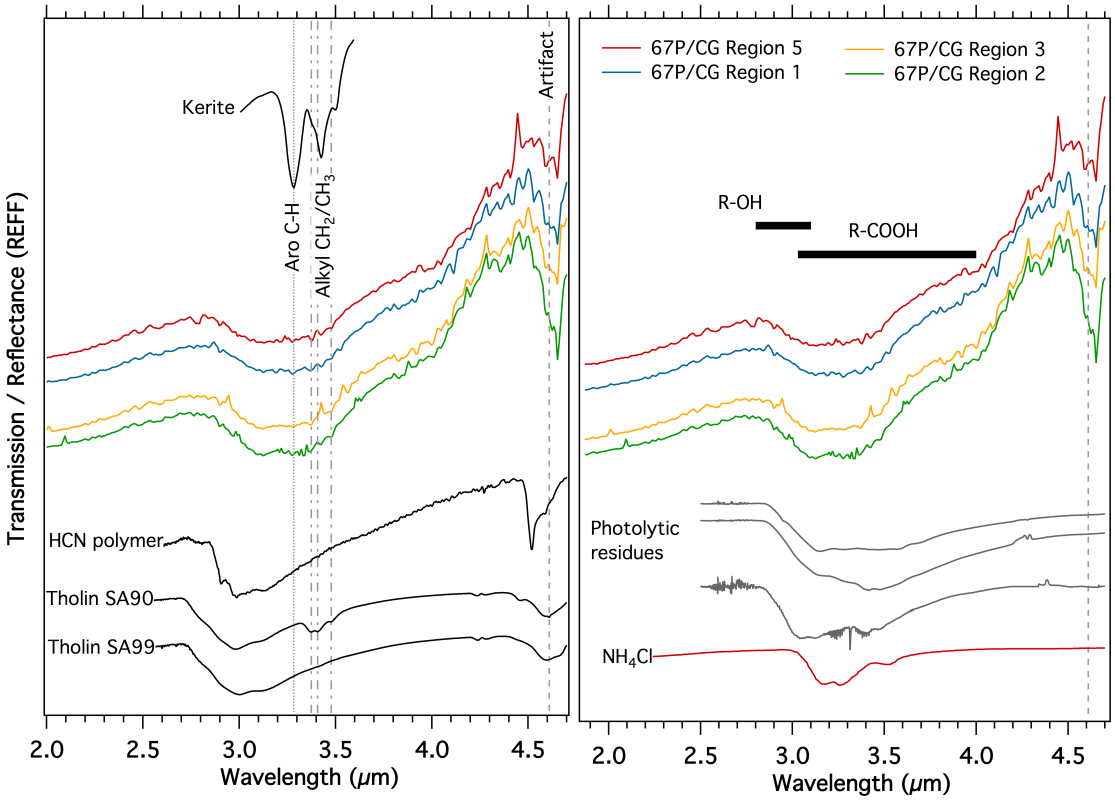


Figure 12: Left: Spectra of 67P/CG plotted with low anthraxolite reflectance spectrum (Moroz et al., 1998), transmission tholins spectra (Quirico et al., 2008), and a HCN polymer spectrum (Bonnet et al., 2015). Spectra are vertically shifted for clarity. The slight shift of the position of the aliphatic modes in the low anthraxolite with respect to those of the tholin SA90 (mixed lines) is due to the nitrogen content. The dotted line points to the position of the 4.6 µm artifact, which also fits with the position of the OCN^- ion in laboratory experiments. Right: Spectra of 67P/CG plotted along with transmission spectra of ammonium salt (NIST database) and of photolytic residues produced under varying conditions (Munoz Caro and Schutte 2003). The ammonium ion appears as a viable candidate, while photolytic residues may display a broad feature that encompasses the 3.2 µm band.

5.3.4 Ammonium ion and photolytic residues

Ammonium ion NH_4^+ appears also as a viable candidate to explain the presence of the 3.2 µm band. This ion is strongly suspected to be present in interstellar ices as a counter-ion of isocyanide OCN^-, which has been identified in different protostars environment through its narrow CN vibration at 2170 cm^{-1} (e.g. Grim and Greenberg, 1987; Schutte and Khanna, 2003). The couple (NH_4^+, OCN^-) has been also identified in numerous experimental simulations that aimed at mimicking organic complexification in the conditions of interstellar molecular clouds or protostars envelopes. In these experiments, simple ices mixtures are irradiated by UV photons, energetic ions or simply evolve by thermal activation (Grim et al., 1989a,b; Schutte and Khanna, 2003; Theule et al., 2013). NH_4^+ and OCN^- are detected in the residues formed after heating to room temperature, and so might be stable at the surface of 67P/CG. Note that in section 5.3.2, we pointed out that the N/C ratio measured in interplanetary dust is low, which points to a very low or negligible contribution of cyanides (-CN) groups. This low abundance mostly concerns refractory organics, while here ions are suspected to be present as a semi-volatile component that is likely absent or extremely weak in dusts.

Ammonium salts display a broad and structured band that extends from ~ 2.94 to ~ 3.34 µm with peaks at 3.17, 3.26, and another peak at 3.51 µm, assigned to the $2\nu_2$, $\nu_1+\nu_5$ and $2\nu_4$ vibration modes, respectively (Fig. 12). In those experiments, NH_4^+ appears early in

the irradiation process. Increasing the irradiation dose leads to more refractory organic films that contain a variety of compounds including carboxylic acid and salts, esters and amides (Munoz-Caro and Schutte, 2003). Such complex mixture causes broader bands than that of a simple ammonium salt, whose broadness fits or even encompasses that of the 3.2 µm band of 67P/CG (Fig. 12). In addition, we have compared in this study laboratory transmission spectra with surface reflectance spectra (Fig. 12). In this respect, we expect a slight broadening and shape modification of the band observed in transmission spectra, because of scattering of photons within the surface particles. Nevertheless, the band structure and position in the transmission spectra can be directly compared to those of reflectance spectra.

The OCN^- ion has a stretching band centered at ~ 4.6 µm. This wavelength falls in the spectral range dominated by the thermal emission of 67P/CG surface. After subtraction of (most of) the thermal component an artifact feature appears at ~4.61 µm in each averaged spectrum computed across each colored area (Fig. 12). The presence of this feature precludes the seek of OCN^-.

5.3.5 Summary

The survey of the plausible species that might account for the 3.2 µm band is summarized in Table 4. The 3.2 µm feature cannot be fitted with a single species and certainly results from the contribution of a variety of molecular and ionic species. Amino groups are minor contributors, if any, while carboxylic groups COOH, alcoholic OH, the ion NH_4^+ and possibly aliphatic and/or aromatic groups CH, CH_2 and CH_3 are strongly suspected. The broadness of the feature suggests the presence of COOH groups tightly connected to promote hydrogen bond interaction. Therefore, COOH groups attached to macromolecular polyaromatic structures causing low reflectance of the cometary nucleus in the visible, can contribute to the 3.2-µm feature but such COOH groups are unlikely the sole COOH carriers of this broad band. Our preferred interpretation is the presence of a molecular/ionic residue as the leftover of ice mixtures exposed to energetic processing in a pre-accretion sequence. As discussed above, several experimental simulations published so far have clearly evidenced the formation of anions and counter-ions (e.g. NH_4^+, OCN^-, etc.) and complex array of molecular species including carboxylic acids. In this respect, VIRTIS data point to a semi-volatile organic component that is not sampled by interplanetary dust, which mostly contains refractory organics (stratospheric IDPs and Antarctic micrometeorites).

	3.2 µm band plausible carrier ?	**Comments**
CH_2/CH_3	+	Plausible.
NH/NH_2	---	Poorly plausible.
-OH in R-COOH	++	Highly plausible, sole candidate that may account for absorption over a broad spectral range and towards longer wavelengths.
-OH in R-OH	+	Plausible. But low abundance if present.
OH in silicates	---	Poorly plausible. Main feature is centered at 2.7-2.8 µm, far outside the range of the 3.2 µm band.
NH_4^+	+	Plausible. Fits nicely the short-wavelength edge of the 3.2 µm band.

Table 4: Species evaluated as possible carrier of the 3.2 μm band. ++: highly plausible. +: plausible. ---: not or poorly plausible.

5.4 Surface processing and rejuvenation, connection to carbonaceous chondrites

The spectrum of 67P/CG does not fit experimental spectra of CI, CM and CR chondrites. The analysis of interplanetary dust particles, Antarctic micrometeorites and Stardust grains sampled in the coma of comet Wild 2 show that comets contain crystalline minerals that were formed in the inner Solar Nebula, and transported in the outer and cold regions through efficient inward-outward transport mechanisms (Zolensky et al., 2006). Radial transfers in the protosolar disk were also operated by planetesimals, triggered by the migration of giant planets (Walsh et al., 2011). The lack of clear distinction of a hot place formation for asteroids, and a cold place formation for comets, led to the emergence of the so-called asteroid-comet continuum concept (Gounelle et al., 2008). Within this framework, the Orgueil CI chondrite has been proposed to originate from a Jupiter Family comet (Gounelle et al., 2006). This cometary origin is not supported by our data, i.e. the mismatch of the CI, CM and CR chondrites spectra (including Orgueil) with those of comet 67P/CG. However, any direct spectral comparison might be misleading due to effects of space weathering, which possibly modified the surface of 67P/CG. Low energy (0.84 keV/amu) ions of solar wind plasma from expanding solar corona continuously bombard the surfaces of solar system objects that are not protected by an atmosphere and/or a magnetic field. Below, we discuss the effect of solar wind irradiation and show that its impact is very weak or absent on comet 67P/CG.

The exposition duration to solar wind of 67P/CG surface controls the irradiation dose. Therefore a key issue lies in the extent, if any, of surface rejuvenation at each perihelion, which would limit this duration to the orbital period (6.44 years). 67P/CG has been selected because its perihelion decreased suddenly in 1959, enhancing chances to get a recently refreshed surface. Dynamical simulations show that the perihelion is located at q=1.2 AU since 1959, and ranged between 2.9 and 3.8 AU until ~200 years ago (Groussin et al., 2007; Maquet, 2015). However, beyond ~200 years, a probabilistic approach is required to perform calculations and some clones in those calculations have very low q. As such, no conclusions are provided by dynamical calculations. OSIRIS observations, along with the analysis of VIRTIS spectral images, provide firmer conclusions on space weathering effect (Sierks et al., 2015). The terrains sampled by the five colored regions presented in section 2 (see Fig. 2) correspond to various morphologies including the (1) rocky consolidated terrains and (2) dust-dominated smooth terrains, and in particular fresh deposits in the lobe (El-Maarry et al. (2015). OSIRIS data point to material mobilization at the surface through, mostly an "airfall" process controlled by dust emission in the Hapi (neck) region associated to a size-sorting process that favors large (~ cm) particles, that are eventually spread out throughout the surface (Thomas et al., 2015). Our analysis of VIRTIS data shows that the 3.2 µm band is ubiquitous in those regions, whatever their morphology and their age (Fig. 2). The spectral variations of the 3.2 µm band are mostly observed between the neck and other regions, and interpreted here as a weak contribution of water ice absorption (Fornasier et al., 2015; De Sanctis et al., 2015). In this respect, the impact of solar wind irradiation is expected to be very limited, and the characteristic irradiation duration lies around 6.44 years for those terrains that are renewed at each perihelion.

However, the detection of refractory elements Na, K, Si and Ca in the coma points to sputtering processes at the surface (Wurz et al., 2015). This detection is not in contradiction with the lack of spectral variation between fresh and old terrains, if the penetration depth of solar wind ions is much smaller than the optical path of photons and/or the defects density induced by implantation within this layer is weak. The effects of solar wind irradiation, on the reflectance spectrum of the CM chondrite Murchison, were experimentally simulated by Lantz et al. (2015). These experiments did not reveal significant spectral modifications in the visible and the near-infrared ranges, for irradiation with 40 keV He+ and Ar+ ions, and equivalent doses up to ~ 7000 years at 3 AU. Interestingly, He^+ irradiation with a fluence of 3

x 10^{16} ions cm^{-2} does not produce significant modifications of the 2.7 µm feature controlled by OH in serpentines, nor in the CH_2/CH_3 vibrations mode at 3.4 µm. Due to saturation effects, further increase of laboratory ion fluence is not expected to cause further optical alteration (Moroz et al., 2004, Brunetto et al. 2004). Solar wind flux is strongly dominated (~96%) by 1 keV protons, which due to their low mass produce less significant radiation damage to carbonaceous chondrite materials, compared to much less abundant heavier ions like 40 keV Ar+ (Moroz et al., 2004).

Radiation damage due to low energy ions is limited to a very thin layer, whose thickness depends on the mass and energy per nucleon of impinging particles, and to a lesser extent on the nature of the target. This thickness lies around a few hundreds of nm for particles with an energy/nucleon of a few 10 keV, and tens of nm for particles of a few keV (Moroz et al., 2004). Within the layer, dramatic effects are observed on the structure (amorphization) and the composition (destruction of C-H and O-H bonds by dehydrogenation). The amorphisation of carbonaceous matter (and likely its dehydrogenation) is observed in this layer in the experiments of Lantz et al. (2015), but they are undetected in the reflectance spectra.

Finally, the typical irradiation duration in fresh deposits is around 6 years. Rough estimates of expected timescales reported by Kanuchova et al. (2012) and Brunetto et al. (2014) suggest that the time to reach on the comet the degree of ion-induced material modifications achieved in laboratory experiments exceeds by orders of magnitude this time scale.

We conclude that the effect of space weathering on the observed 3.2 µm band is negligible, and those effects would be also negligible if the cometary surface was composed of hydrated minerals that display a 2.7 µm band. The lack of connection between 67P/CG and CI, CM and CR chondrites is a firm result. Solar wind sputtering and implantation happen at the surface of 67P/CG, as testified by the presence of refractory atoms in the coma. However, this irradiation is limited to a very shallow depth (< ~100 nm), did not attain a saturation regime (low defects density) and do not lead to spectroscopic effects on the 3.2 µm band.

CONCLUSION

The main conclusions of this manuscript are the following:

1. The low albedo of comet 67P/CG, as well as its reddish slope in the visible, are controlled by a dark refractory polyaromatic carbonaceous component mixed up with opaque minerals. VIRTIS data do not provide direct insights into the nature of these opaque minerals. However, according to the composition of cometary grains analyzed in the laboratory, we infer the most likely candidates are ~FeS sulfides and Fe-Ni alloys.
2. A semi-volatile component, consisting of a complex mixture of low weight molecules not volatilized at T < 220 K, is a carrier of the 3.2 μm band. Water ice has likely a significant contribution in the neck region, and a weak or negligible one in other regions.
3. The 3.2 μm band is likely the contribution of several chemical groups. The OH group in carboxylic acids appears as a highly plausible candidate as it can encompass the full broadness of the band. The ion NH_4^+ is likewise plausible.
4. Photolytic/thermal residues, produced in laboratory from interstellar ice analogs, which are complex mixtures of low weight molecules and ions, can be fair spectral

analogs. In this respect, the 3.2 μm band may testify of nebular or interstellar chemistry.

5. No hydrated minerals were identified and our data support the lack of genetic links with the CI, CR and CM primitive chondrites. This concerns in particular the Orgueil chondrite, which had been suspected to have a cometary origin.

ACKNOWLEDGEMENTS

We thank the following institutions and agencies, which supported this work: Italian Space Agency (ASI - Italy), Centre National d'Etudes Spatiales (CNES- France), Deutsches Zentrum für Luft- und Raumfahrt (DLR- Germany), National Aeronautic and Space Administration (NASA- USA) Rosetta Program, Science and Technology Facilities Council (UK). VIRTIS has been built by a consortium, which includes Italy, France and Germany, under the scientific responsibility of the Istituto di Astrofisica e Planetologia Spaziali of INAF, Italy, which guides also the scientific operations. The VIRTIS instrument development has been funded and managed by ASI, with contributions from Observatoire de Meudon financed by CNES, and from DLR. The computational resources used in this research have been supplied by INAF-IAPS through the DataWell project. Université Grenoble Alpes (UGA) and CNES are warmly awarded for their support to instrumental facilities and activities at IPAG. We warmly thank Jean-Noël Rouzaud (ENS Paris - France) for having provided us with coal tar samples, and Arnaud Buch (Ecole Centrale de Paris) for having performed the elemental analysis of these samples. Emmanuel Dartois and Rosario Brunetto are warmly thanked for fruitful and stimulating discussions on ion irradiation and space weathering, and George Flynn for stimulating discussions on the connection between stratospheric IDPs and comets. Guillermo Munoz-Caro is warmly thanked for having provided electronic files of photolytic residues and for stimulating discussions on their synthesis. We thank Gilles Montagnac and the Raman National Facility at Ecole Normale Supérieure de Lyon where Raman analyses were done. L.V.M. acknowledges the DFG grant MO 3007/1-1. Mathilde faure acknowledges a PhD grant from Université Grenoble Alpes.

REFERENCES

Aleon, J., Engrand, C., Robert, F., Chaussidon, M. (2001) Clues to the origin of interplanetary dust particules from the isotopic study of their hydrogen-bearing phases. *Geochim. Cosmochim. Acta***65**, 4399–4412.

Alexander C. M. O. D., Fogel M., Yabuta H. and Cody G. D. (2007) The origin and evolution of chondrites recorded in the elemental and isotopic compositions of their macromolecular organic matter. *Geochim. et Cosmochim. Acta*. **71,** 4380-4403.

Beck P., Quirico E., Montes-Hernandez G., Bonal L., Bollard J., Orthous-Daunay F.-R., Howard K.T., Schmitt B., Brissaud O., Deschamps F., Wunder B., and Guillot S. (2010) Hydrous mineralogy of CM and CI chondrites from infrared spectroscopy and their relationship with low albedo asteroids. *Geochim. Cosmochim. Acta* **74**, 4881-4892.

Beck P., Quirico E., Sevestre D., Montes-Hernandez G., Pommerol A. and Schmitt B. (2011) Goethite as an alternative origin of the 3.1 μm band on dark asteroids. *Astro. Astroph.* **526**, A85

Berthelot M.P.E. (1868) Sur la matière charbonneuse des météorites. *Comptes rendus hebdomadaires des séances de l'académie des sciences* **67**, 849

Bither T.A., Bouchard R.J., Cloud W.H., Donohue P.C. and Siemons W.J. (1968) Transition metal pyrite dichalcogenites. High-pressure synthesis and correlation of properties. *Inorg. Chem.* **7**, 2208-2220

Bonal L., Quirico E. and Bourot-Denise (2006) Determination of the petrologic type of CV3 chondrites by Raman spectroscopy of included organic matter. *Geochim. Cosmochim. Acta*. **70,** 1849-1863.

Bonal L., Quirico E. and Montagnac G. (2011). Structure of primitive polyaromatic carbonaceous matter: IDPs vs. Chondrites. *Met. Plan. Sci*. Abstract #5125

Bonnefoy N. (2001) Développement d'un spectrophoto-goniomètre pour l'étude de la réflectance bidirectionnelle des surfaces géophysiques. Application au soufre et perspectives pour le satellite Io. *Thèse* Université Joseph Fourier, Grenoble.

Brissaud O., Schmitt B., Bonnefoy N., Douté S., Rabou P., Grundy W. and Fily M. (2014) Spectrogonio Radiometer for the Study of the Bidirectional Reflectance and Polarization Functions of Planetary Surfaces. 1. Design and Tests. *Applied Optics* **43**, 1926-1937

Britt D.T., Bell J.F., Haack H. and Scott E.R.D. (1992) The reflectance spectrum of troilite. *Lunar and Planetary Science Conference* (Abstr.).

Brunetto R., Pino T., Dartois E., Cao A-T, d'Hendecourt L., Strazzulla G. and Brechignac P. (2009) Comparison of the Raman spectra of ion irradiated soot and collected extraterrestrial carbon. *Icarus***200**, 323-337

Brunetto R., C. Lantz, D. Ledu, D. Baklouti, M.A. Barucci, P. Beck, L. Delauche, Z. Dionnet,

P. Dumas, J. Duprat, C. Engrand, F. Jamme, P. Oudayer, E. Quirico, C. Sandt, E. Dartois (2014) Ion irradiation of Allende meteorite probed by visible, IR, and Raman spectroscopies. *Icarus* **237**, 278-292

Busemann H., Nguyen A. N., Cody G. D., Hoppe P., Kilcoyne A. L. D., Stroud R. M., Zega T. J. and L. R. Nittler (2009) Ultra-primitive interplanetary dust particles from the comet 26P/Grigg-Skjellerup dust stream collection. *Earth Planet. Sci. Lett.* **288,** 44-57.

F. Capaccioni, A. Coradini, G. Filacchione, S. Erard, G. Arnold, P. Drossart, M. C. De Sanctis, D. Bockelee-Morvan, M. T. Capria, F. Tosi, C. Leyrat, B. Schmitt, E. Quirico, P. Cerroni, V. Mennella, A. Raponi, M. Ciarniello, T. McCord, L. Moroz, E. Palomba, E. Ammannito, M. A. Barucci, G. Bellucci, J. Benkhoff, J. P. Bibring, A. Blanco, M. Blecka, R. Carlson, U. Carsenty, L. Colangeli, M. Combes, M. Combi, J. Crovisier, T. Encrenaz, C. Federico, U. Fink, S. Fonti, W. H. Ip, P. Irwin, R. Jaumann, E. Kuehrt, Y. Langevin, G. Magni, S. Mottola, V. Orofino, P. Palumbo, G. Piccioni, U. Schade, F. Taylor, D. Tiphene, G. P. Tozzi, P. Beck, N. Biver, L. Bonal, J.-Ph. Combe, D. Despan, E. Flamini, S. Fornasier, A. Frigeri, D. Grassi, M. Gudipati, A. Longobardo, K. Markus, F. Merlin, R. Orosei, G. Rinaldi, K. Stephan, M. Cartacci, A. Cicchetti, S. Giuppi, Y. Hello, F. Henry, S. Jacquinod, R. Noschese, G. Peter, R. Politi, J. M. Reess, A. Semery (2015) The organic-rich surface of comet 67P/Churyumov-Gerasimenko as seen by VIRTIS/Rosetta. *Science* **347**, 628-1-4

Castiglioni C., Mapelli C., Negri F. and Zerbi G (2001) Origin of the D line in the Raman spectrum of graphite: A study based on Raman frequencies and intensities of polycyclic aromatic hydrocarbon molecules. *J. Chem. Phys*. **114**, 963-974

M. Ciarniello, F. Capaccioni, G. Filacchione, A. Raponi, F. Tosi, M. C. De Sanctis, M. T. Capria, S. Erard, D. Bockelee-Morvan, C. Leyrat, G. Arnold, A. Barucci, P. Beck, G. Bellucci, S. Fornasier, A. Longobardo, S. Mottola, E. Palomba, E. Quirico and B. Schmitt (2015) Photometric properties of comet 67P/Churyumov-Gerasimenko from VIRTIS-M onboard Rosetta. *Astron. Astroph*. In press

Cloutis E. A., Gaffey M. J. and Moslow T. F. (2015) Spectral reflectance properties of carbon-bearing materials (1994) *Icarus* **107**, 276-287

Coradini A., F. Capaccioni, P. Drossart, G. Arnold, E. Ammannito, F. Angrilli, A. Barucci, G. Bellucci, J. Benkhoff, G. Bianchini, J. P. Bibring, M. Blecka, D. Bockelee-Morvan, M. T. Capria, R. Carlson, U. Carsenty, P. Cerroni, L. Colangeli, M. Combes, M. Combi, J. Crovisier, M. C. Desanctis, T. Encrenaz, S. Erard, C. Federico, G. Filacchione, U. Fink, S. Fonti, V. Formisano, W. H. Ip, R. Jaumann, E. Kuehrt, Y. Langevin, G. Magni, T. McCord, V. Mennella, S. Mottola, G. Neukum, P. Palumbo, G. Piccioni, H. Rauer, B. Saggin, B. Schmitt, D. Tiphene and G. Tozzi (2007) VIRTIS : an imaging spectrometer for the ROSETTA mission. *Space Sci. Rev*. **128**, 529-559

Dartois E., Engrand C., Brunetto R., Duprat J., Pino T., Quirico E., Rémusat L., Bardin N., Briani G., Mostefaoui S., Morinaud G., Crane B., Szwec N., Delauche L., Jamme F. and Sandt Ch. (2013) Ultracarbonaceous Antarctic micrometeorites, probing the Solar System beyong the nitrogen snow line. *Icarus* **234**, 243-252

De Bergh C., Schmitt B., Moroz L.V., Quirico E. and Cruikshank D.P. (2008) Laboratory data on ices, refractory carbonaceous materials, and minerals relevant to transneptunian

objects and centaurs. In The Solar System Beyond Neptune (eds A. Barucci, H. Boehnhardt, D. Cruikshank, A. Morbidelli), pp. 483-506. *Arizona University Press: Tucson.*

De Sanctis M.C., F. Capaccioni, M. Ciarniello, G. Filacchione, M. Formisano, S. Mottola, A. Raponi, F. Tosi, D. Bockelée-Morvan, S. Erard, C. Leyrat, B. Schmitt, E. Ammannito, G. Arnold, M. A. Barucci, M. Combi, M. T. Capria, P. Cerroni, W.-H. Ip, E. Kuehrt, T. B. McCord, E. Palomba, P. Beck, E. Quirico & The VIRTIS Team (2015) The diurnal cycle of water ice on comet 67P/Churyumov–Gerasimenko. *Nature* **525**, 500-503

Derenne S., Rouzaud J-N, Clinard C. and Robert F. (2005) Size discontinuity between interstellar and chondritic aromatic structures: a high-resolution transmission électron microscopy study. *Geochim. Cosmochim. Acta* **69**, 3911-3918

Dobrica, E., Engrand C., Duprat J., Gounelle M., Leroux H., Quirico E. and Rouzaud J.-N. (2009) Connection between micrometeorites and Wild 2 particles from Antarctic snow to cometary ices. *Met. Plan. Sci.* **44**, 1643-1661

Dobrica E., Engrand C., Quirico E., Montagnac G. and Duprat J. (2011) Raman characterization of carbonaceous matter in CONCORDIA Antarctic micrometeorites. *Met. Planet. Spa. Sci.* **46**, 1363-1375.

El-Maarry M. R., N. Thomas, L. Giacomini, M. Massironi, M. Pajola, R. Marschall, A. Gracia-Berná, H. Sierks, C. Barbieri, P. L. Lamy, R. Rodrigo, H. Rickman, D. Koschny, H. U. Keller, J. Agarwal, M. F. A'Hearn, A-T. Auger, M. A. Barucci, J-L. Bertaux, I. Bertini, S. Besse, D. Bodewits, G. Cremonese, V. Da Deppo, B. Davidsson, M. De Cecco, S. Debei, C. Güttler, S. Fornasier, M. Fulle, O. Groussin, P. J. Gutierrez, S. F. Hviid, W-H. Ip, L. Jorda, J. Knollenberg, G. Kovacs, J.-R. Kramm, E. Kührt, M. Küppers, F. La Forgia, L. M. Lara, M. Lazzarin, J. J. Lopez Moreno, S. Marchi, F. Marzari, H. Michalik, G. Naletto, N. Oklay, A. Pommerol, F. Preusker, F. Scholten, C. Tubiana, and J-B. Vincent (2015). *Astron. Astroph.* **583**, A26

Ferrari A. C. and Robertson J. (2001) Resonant Raman spectros- copy of disordered, amorphous, and diamond like carbon. Phys. Rev. B 64, 075414.

Filacchione G., M. C. De Sanctis, F. Capaccioni, A. Raponi, F. Tosi, M. Ciarniello, P. Cerroni, G. Piccioni, M. T. Capria, E. Palomba, G. Bellucci, S. Erard, D. Bockelee-Morvan, C. Leyrat, G. Arnold, M. A. Barucci, M. Fulchignoni, B. Schmitt, E. Quirico, R. Jaumann, K. Stephan, A. Longobardo, V. Mennella, A. Migliorini, E. Ammannito, J. Benkhoff, J. P. Bibring, A. Blanco, M. Blecka, R. Carlson, U. Carsenty, L. Colangeli, M. Combes, M. Combi, J. Crovisier, P. Drossart, T. Encrenaz, C. Federico, U. Fink, S. Fonti, W. H. Ip, P. Irwin, E. Kuehrt, Y. Langevin, G. Magni, T.McCord, L. Moroz, S. Mottola, V.Orofino, P. Palumbo, U. Schade, F. Taylor, D. Tiphene, G. P. Tozzi, P. Beck, N. Biver, L. Bonal, J-Ph. Combe, D. Despan, E. Flamini, S. Fornasier, A. Frigeri, D. Grassi, M. Gudipati, F. Mancarella, K. Markus, F. Merlin, R. Orosei, G. Rinaldi, M. Cartacci, A. Cicchetti, S. Giuppi, Y. Hello, F. Henry, S. Jacquinod, J. M. Reess, R. Noschese, R. Politi, G. Peter (2015). Exposed water ice in bright albedo patches in the Imhotep region of comet 67P/CG. *Nature*, in press

Fornasier, S., Hasselmann, P. H., Barucci, M. A., Feller, C., Besse, S., Leyrat, C., Lara, L., Gutierrez, P. J., Oklay, N., Tubiana, C., Scholten, F., Sierks, H., Barbieri, C., Lamy, P. L., Rodrigo, R., Koschny, D., Rickman, H., Keller, H. U., Agarwal, J., A'Hearn, M. F., Bertaux, J.-L., Bertini, I., Cremonese, G., Da Deppo, V., Davidsson, B., Debei, S., De Cecco, M., Fulle, M., Groussin, O., Gu¨ttler, C., Hviid, S. F., Ip, W., Jorda, L., Knollenberg, J., Kovacs, G., Kramm, R., Ku¨hrt, E., Ku¨ppers, M., La Forgia, F., Lazzarin, M., Lopez Moreno, J. J., Marzari, F., Matz, K.-D., Michalik, H., Moreno, F., Mottola, S., Naletto, G., Pajola, M., Pommerol, A., Preusker, F., Shi, X., Snodgrass, C., Thomas, N., and Vincent, J.-B. (2015). Spectrophotometric properties of the nucleus of comet 67P/Churyumov-Gerasimenko from the OSIRIS instrument onboard the ROSETTA spacecraft. eprint arXiv:1505.06888. *Astronomy and Astrophysics* **583**, A30

Flynn G. J., Keller L. P., Feser M. Wirick S. and Jacobsen C. (2003) The origin of organic matter in the solar system: evidence from the interplanetary dust particles. *Geochim. Cosmochim. Acta.* **67,** 4791-4806.

Gardinier A., Derenne S., Robert F., Behar F., Largeau C and Maquet J. (2000) Solid state CP/MAS C-13 NMR of the insoluble organic matter of the Orgueil and Murchison meteorites: Quantitative study. *Earth Planet. Sci. Lett*. **184,** 9-21.

Garenne A., P. Beck, G. Montes-Hernandez, O. Brissaud, B. Schmitt, E. Quirico, L. Bonal, C. Beck, K.T. Howard (2015) What is controlling the reflectance spectra of carbonaceous chondrites? *Icarus,* In press.

Gounelle M. and Zolensky M.E. (2001) A terrestrial origin for sulfate veins in CI1 chondrites. *Met. Plan. Sci.* **36**, 1321-1329

Gounelle M., Morbidelli A., Bland P. A., Sephton M. A., Young E. D., and Spurny P. (2008) Meteorites from the outer solar system? In The Solar System Beyond Neptune (eds A. Barucci, H. Boehnhardt, D. Cruikshank, A. Morbidelli), pp. 525-541. *Arizona University Press: Tucson.*

Gounelle M., Spurny P., and Bland P. A. (2006) The atmospheric trajectory and orbit of the Orgueil meteorite. *Meteoritics Planet. Sci*. **41**, 135-150.

Groussin O., Hahn G., Lamy P.L., Gonczi R. and Valsecchi G.B. (2007) The long-term evolution and initial size of comets 46P/Wirtanen and 67P/Churyumov-Gerasimenko. *Mon. Not. R. Astron. Soc*. **376**, 1399-1406

Grim R.J.A., and J.M. Greenberg (1987) *Astrophys. J.* **321**, L91.

Grim, R.J.A., J.M. Greenberg, W. Schutte, and B. Schmitt (1989a) Ions in grain mantles: II. A new explanation for the 6.86 μm absorption in W33A. *Astrophys. J.* **341,** L87-L90

Grim, R.J.A., J.M. Greenberg, M.S. de Groot, F. Baas, W.A. Schutte, and B. Schmitt (1989b) Infrared Spectroscopy of Astrophysical Ices: New insights in the Photochemistry. *Astron. Astrophys. Suppl. Ser.*, **78,** 161-186

Hapke B. (1993) Theory of Reflectance and Emittance Spectroscopy, *Cambridge Univ. Press*.

Hughes A. L. H. and Armitage P. J. (2010). Particle transport in evolving protoplanetary disks : implications for results from STARDUST. *Astroph. J*. **719**, 1633-1653

Kanuchova Z., Baratta G.A., Garozzo M. and Strazzulla G. (2010) Space weathering of asteroidal surfaces. *Astro. Astroph*. **517**, A60

Kanuchova K., Brunetto R., Melita M. and Strazzulla G. (2012) Space weathering and the color indexes of minor bodies in the outer solar system. *Icarus* **221**, 12-19

Kebukawa Y., Alexander C. M. O'D. and Cody G. D. (2011) Compositional diversity in insoluble organic matter in type 1, 2 and 3 chondrites as detected by infrared spectroscopy. *Geochim. Cosmochim. Acta*. **75,** 3530-3541.

Keller L. P., Messenger S., Flynn G. J., Clemett S., Wirick S. and Jacobsen C. (2004) The nature of molecular cloud material in interplanetary dust. *Geochim. Cosmochim. Acta*. **68,** 2577-2589.

Kerridge J. F. (1999) Formation and processing of organics in the early solar system. *Space Sci. Rev.* **90,** 275–288.

Lair V., Antony H., Legrand L. and Chaussé A. (2006) Electrochemical reduction of ferric corrosion products and evaluation of galvanic coupling with iron. *Corrosion science* **48**, 2050, 2063

Lantz C., Brunetto R., Barucci M.A., Dartois E., Duprat J., ENgrand C., Godard M., Ledu D. and Quirico E (2015). Ion irradiation of the Murchison meteorite: visible to mid-infrared spectroscopic results. *Astro. Astroph.* **577**, A41

Leroux H., Rietmeijer F.J.M., Velbel M.A., Brearley A. J., Jacob D., Langenhorst F., Bridges J.C., Zega T.J., Stroud R.M., Cordier P., Harvey R.P., Lee M., Gounelle M., Zolensky M.E. (2008) A TEM study of thermally modified comet 81P/Wild 2 dust particles by interactions with the aerogel matrix during the Stardust capture process. *Met. Plan. Sci*. **43**, 97-120

Lin-Vien, D., Colthup, N.B., Fateley, W.G., Grasselli, J.G., 1991. The Handbook of In- frared and Raman Characteristic Frequencies of Organic Molecules. Academic Press, San Diego, 503 pp.

Lynch D. W. and Hunter W. R. (1991) Handbook of Optical Constants of Solids II, *Academic Press.*

Maquet L. (2015) The recent dynamical history of comet 67P/Churyumov-Gerasimenko. *Astron. Astroph*. **579**, A78

Matrajt G., Munoz Caro G.M., Dartois E., d'Hendecourt L., Deboffle and Borg J. (2005) FTIR analysis of the organics in IDPs: Comparison with the IR spectra of the diffuse interstellar medium. *Astro. Astroph*. **433**, 979-995

1128 Merouane S., Djouadi Z. and Le Sergeant d'Hendecourt L. (2014) Relations between
1129 aliphatics and silicate components in 12 stratospheric particles deduced from vibrational
1130 spectroscopy. *Ap. J.* **780**, 174
1131
1132 Mewaldt R.A., Cohen C.M.S., Mason G.M., Haggerty D.K. and Desai M.I. (2007) Long-term
1133 fluences of solar energetic particles from H to Fe. *Space Sci. Rev*. **130**, 323-328
1134
1135 Moroz L.V., Arnold G., Korochantsev A.V. and Wäsch R. (1998) Natural bitumens as
1136 possible analogs for cometary and asteroid organics : 1. Reflectance spectroscopy of pure
1137 bitumens. *Icarus* **134**, 253-268
1138
1139 Moroz L., Baratta G., Strazzulla G., Starukhina L., Dotto E., Barucci M.A., Arnold G. and
1140 Distefano E. (2004) Optical alteration of complex organics induced by ion irradiation : 1.
1141 Laboratory experiments suggest unusual space weathering trend. *Icarus* **170**, 214-228
1142
1143 Moroz L.V., Schmidt M., Schade U., Hiroi T. and Ivanova M.A. (2006) Synchrotron-based
1144 infrared microspectroscopy as a useful tool to study hydration states of meteorite constituents.
1145 *Met. Plan. Sci*. **41**, 1219-1230
1146
1147 Munoz Caro G.M. and Schutte W.A. (2003) UV-photoprocessing of interstellar ice analogs :
1148 New infrared spectroscopic results. *Astro. Astroph*. **412**, 121-132
1149
1150 Ogliore R.C., Butterworth A.L., Fakra S.C., Gainsforth Z., Marcus M.A. and Westphal A.J.
1151 (2010) Comparison of the oxidation state of Fe in comet 81P/Wild 2 and chondritic-porous
1152 interplanetary dust particles. *Earth Plan. Sci.Lett*. **296**, 278-286
1153
1154 Ordal M. A., Long L. L., Bell R.J., Bell S.E., Bell R.R., Alexander Jr. R.W and Ward C.A.
1155 (1983) Optical properties of the metals Al, Co, Cu, Au, Fe, Pb, Ni, Pd, Pt, Ag, Ti, and W in
1156 the infrared and far infrared. *Applied optics* **22**, 1099-1120
1157
1158 Orthous-Daunay F.R., Quirico E., Beck P., Brissaud O., Dartois E., Pino T. and Schmitt B.
1159 (2013) Mid-infrared study of the molecular structure variability of insoluble organic matter
1160 from primitive chondrites. Icarus **223**, 534-543
1161
1162 Pommerol A., N. Thomas, M. R. El-Maarry, M. Pajola, O. Groussin, A. -T. Auger, N. Oklay,
1163 S. Fornasier, C. Feller, B. Davidsson, A. Gracia-Berná, B. Jost, R. Marschall, O. Poch, M. A.
1164 Barucci, J. -L. Bertaux, F. La Forgia, H. U. Keller, E. Kührt, S. C. Lowry, S. Mottola, G.
1165 Naletto, H. Sierks, C. Barbieri, P. L. Lamy, R. Rodrigo, D. Koschny, H. Rickman, J. Agarwal,
1166 M. F. A'Hearn, I. Bertini, S. Boudreault, G. Cremonese, V. Da Deppo, M. De Cecco, S.
1167 Debei, C. Güttler, M. Fulle, P. J. Gutierrez, S. F. Hviid, W. -H. Ip, L. Jorda, J. Knollenberg,
1168 G. Kovacs, J. -R. Kramm, E. Küppers, L. Lara, M. Lazzarin, J. L. Lopez Moreno, F. Marzari,
1169 H. Michalik, F. Preusker, F. Scholten, C. Tubiana, and J. -B. Vincent (2015) OSIRIS
1170 observations of meter-sized exposures of H2O ice at the surface of 67P/Churyumov-
1171 Gerasimenko and interpretation using laboratory experiments. *Astro. Astrophys* **583**, A25

1172 Quirico E., Montagnac G., Rouzaud J.-N., Bonal L., Bourot-Denise M., Duber S., and
1173 Reynard B. (2009) Precursor and metamorphic conditions effects on Raman spectra of
1174 poorly-ordered carbonaceous matter in chondrites and coals. *Earth Plan. Sci. Letters* **287**,
1175 185-193.
1176

Quirico E., Montagnac G., Lees V., McMillan P. F., Szopa C., Cernogora G., Rouzaud J-N, Simon P., Bernard J-M, Coll P., Fray N., Minard R. D., Raulin F., Reynard B. and Schmitt B. (2008) New experimental constraints on composition and structure of tholins. *Icarus***198**, 218-231.

Quirico, E., Borg J., Raynal P-I, Montagnac G. and d'Hendecourt L. (2005) A micro- Raman survey of 10 IDPs and 6 carbonaceous chondrites 2005. *Planet. Space. Sci*. **53**, 1443-1448.

Remusat L., Derenne S. and Robert F. (2005) New insight on aliphatic linkages in the macromolecular organic fraction of Orgueil and Murchison meteorites through ruthenium tetroxide oxidation. *Geochim. Cosmochim. Acta* **69**, 4377-4386

Rietmeijer F. J. M. (1998) Interplanetary dust particles. In Planetary Materials, Reviews in Mineralogy, vol. 36 (ed. J. J. Papike), pp. 2-1–2-95. Planetary Materials, Reviews in Mineralogy. Mineralogical Society of America, Washington, DC.

Robertson J. (1995) Structural models of a-C and a-C :H. *Diam. Rel. Mater*. **4**, 297-301

Schmitt-Koplin P., Gabelica Z., Gougeon R.D., Fekete A., Kanawatu B., Harir M., Gebefuegi I., Eckel G., Hertkorn N. (2010) High molecular diversity of extraterrestrial organic matter in murchison meteorite revealed 40 years after its fall. *Proc. Nation. Acad. Sci*.. **107**, 2763–2768.

Schutte W.A. and Khanna R.K. (2003) Origin of the 6.85 μm band near young stellar objects : the ammonium ion (NH_4^+) revisited. *Astro. Astroph*. **398**, 1049-1062

Sephton M. A. (2002) Organic compounds in carbonaceous chondrites. *Nat. Prod. Rep*. **19**, 292-311

Sierks H., Cesare Barbieri, Philippe L. Lamy, Rafael Rodrigo, Detlef Koschny, Hans Rickman, Horst Uwe Keller, Jessica Agarwal, Michael F. A'Hearn, Francesco Angrilli, Anne-Therese Auger, M. Antonella Barucci, Jean-Loup Bertaux, Ivano Bertini, Sebastien Besse, Dennis Bodewits, Claire Capanna, Gabriele Cremonese, Vania Da Deppo, Björn Davidsson, Stefano Debei, Mariolino De Cecco, Francesca Ferri, Sonia Fornasier, Marco Fulle, Robert Gaskell, Lorenza Giacomini, Olivier Groussin, Pablo Gutierrez-Marques, Pedro J. Gutiérrez, Carsten Güttler, Nick Hoekzema, Stubbe F. Hviid, Wing-Huen Ip, Laurent Jorda, Jörg Knollenberg, Gabor Kovacs, J. Rainer Kramm, Ekkehard Kührt, Michael Küppers, Fiorangela La Forgia, Luisa M. Lara, Monica Lazzarin, Cédric Leyrat, Josè J. Lopez Moreno, Sara Magrin, Simone Marchi, Francesco Marzari, Matteo Massironi, Harald Michalik, Richard Moissl, Stefano Mottola, Giampiero Naletto, Nilda Oklay, Maurizio Pajola, Marco Pertile, Frank Preusker, Lola Sabau, Frank Scholten, Colin Snodgrass, Nicolas Thomas, Cecilia Tubiana, Jean-Baptiste Vincent, Klaus-Peter Wenzel, Mirco Zaccariotto, Martin Pätzold (2015) On the nucleus structure and activity of comet 67P/Churyumov-Gerasimenko. *Science* **347,** 1044-1-5

Starkey, N. A., Franchi, I. A., and Alexander, C. M. O'D. (2013) A Raman spectroscopic study of organic matter in interplanetary dust particles and meteorites using multiple wavelength laser excitation. *Meteoritics and Planetary Science* **48**, 1800-1822

Strazzulla G. and Moroz L. (2005) Ion irradiation of asphaltite as an analogue of solid hydrocarbons in the interstellar medium. *Astro. Astroph.* **434**, 593-598

Theulé P., Duvernay F., Danger G., Borget F., Bossa J.B., Vinogradoff V., Mispelaer F. and Chiavassa T. (2013) *Adv. Space Res*. **52**, 1567-1579

Thomas K. L., Blanford G. E., Keller L. P., Klock W. and McKay D.S. (1993) Carbon abundance and silicate mineralogy of anhydrous interplanetary dust particles. *Geochim. Cosmochim. Acta* **57**, 15551-1566

Thomas N., B. Davidsson, M.R. El-Maarry, S. Fornasier, L. Giacomini, A.G. Gracia-Berná, S.F. Hviid, W.-H. Ip, L. Jorda, H.U. Keller, J. Knollenberg, E. Kührt, F. La Forgia, I.L. Lai, Y. Liao, R. Marschall, M. Massironi, S. Mottola, M. Pajola, O. Poch, A. Pommerol, F. Preusker, F. Scholten, C.C. Su, J.S. Wu, J.-B. Vincent, H. Sierks, C. Barbieri, P.L. Lamy, R. Rodrigo, D. Koschny, H. Rickman, M. F. A'Hearn, M.A. Barucci, J-L. Bertaux, I. Bertini, G. Cremonese, V. Da Deppo, S. Debei, M. de Cecco, M. Fulle, O. Groussin, P.J. Gutierrez, J.-R. Kramm, M. Küppers, L. M. Lara, M. Lazzarin, J. J. Lopez Moreno, F. Marzari, H. Michalik, G. Naletto, J. Agarwal, C. Güttler, N. Oklay and C. Tubiana (2015) Redistribution of particles across the nucleus of comet 67P/Churyumov-Gerasimenko. *Astron. Astroph* **583**, A17

Walsh K.J., Morbidelli A., Raymond S.N., O'Brien D.P. and Mandell A.M. (2011) A low mass for Mars from Jupiter's early gas-driven migration. *Nature* **475**, 206-209

Weaver J.H., Colavita E., Lynch D.W. and Rosei R. (1979) Low-energy interband absorption in bcc Fe and hcp Co. *Phys. Rev. B* **19**, 3850-3856

Wopenka B. (1988) Raman observations on individual interplanetary dust particules. *Earth Planet. Sci. Lett*. **88**, 221-231

Wurz P., Martin Rubin, Kathrin Altwegg, Hans Balsiger, Jean-Jacques Berthelier, André Bieler, Ursina Calmonte, Johan De Keyser, Björn Fiethe, Stephen A. Fuselier, André Galli, Sébastien Gasc, Tamas I. Gombosi, Annette Jäckel, Léna Le Roy, Urs A. Mall, Henri Rème, Valeriy Tenishev and Chia-Yu Tzou (2015) Solar wind sputtering of dust on the surface of 67P/Churyumov-Gerasimenko. *Astron. Astrophys* **583**, A22

Zolensky M. E., Zega, T. J., Yano, H., Wirick S., Westphal A. J., Weisberg M. K., Weber Iris., Warren, J. L., Velbel M. A., Tsuchiyama A., Tsou P., Toppani A., Tomioka N., Tomeoka K., Teslich N., Taheri M., Susini J., Stroud R., Stephan T., Stadermann F. J., Snead C. J., Simon S. B., Simionovici A., See T. H., Robert F., Rietmeijer F. J. M., Rao W., Perronnet M. C., Papanastassiou D. A., Okudaira K., Ohsumi K., Ohnishi I., Nakamura-Messenger K., Nakamura T., Mostefaoui S., Mikouchi T., Meibom A., Matrajt G., Marcus M. A., Leroux H., Lemelle L., Le L., Lanzirotti A., Langenhorst F., Krot A. N., Keller L. P., Kearsley A. T., Joswiak D., Jacob D., Ishii, H., Harvey R., Hagiya K., Grossman L., Grossman J. N., Graham G. A., Gounelle M., Gillet P., Genge M. J., Flynn G., Ferroir T., Fallon S., Ebel D. S., Dai Z. R., Cordier P., Clark B., Chi M., Butterworth A. L., Brownlee D. E., Bridges J. C., Brennan S., Brearley A., Bradley J. P., Bleuet P., Bland P. A. and Bastien R. (2006) Mineralogy and Petrology of Comet 81P/Wild 2 Nucleus Samples. *Science* **314**, 1735